

TALLINN UNIVERSITY OF TECHNOLOGY  
School of Information Technologies

Anar Abdullayev 194246IVEM

# **DSP Based Impedance Spectroscopy Device**

Master's thesis

Supervisor: Olev Martens  
Professor

Tallinn 2021

TALLINNA TEHNIKAÜLIKOOL  
Infotehnoloogia teaduskond

Anar Abdullayev 194246IVEM

# **DSP-põhine impedantsspektroskoopia seade**

Magistriröö

Juhendaja: Olev Märtens  
Professor

Tallinn 2021

## **Author's declaration of originality**

I hereby certify that I am the sole author of this thesis. All the used materials, references to the literature and the work of others have been referred to. This thesis has not been presented for examination anywhere else.

Author: Anar Abdullayev

10.05.2021

## **Abstract**

This thesis project's aim is to research and develop a DSP-based impedance spectroscopy system. The final device includes a custom-built PCB add-on with analog circuits in addition to Texas Instruments TMS320F28379D Dual-Core Microcontroller. Final product was planned to be a versatile, relatively inexpensive, and customizable impedance measurement system that can be used in a variety of applications.

Different impedance spectroscopy methods were studied at the start of this project, and baselines of suitable design for a DSP-based impedance spectroscopy system were implemented. After that, the required parameters and design goals were listed. External components were then chosen to create the PCB board. Since an impedance spectroscopy device was expected to analyse an object's AC response, any DC signal present in the process must be filtered in addition to the high frequency noise. Circuit architecture was iteratively simulated and developed based on high precision measurement and high frequency considerations. Final version of PCB was designed to operate with the set of two different op-amps, then it is fabricated and assembled.

The software design was then implemented based on the initial specifications. It was investigated how to generate binary excitation signals with high resolution PWM, sample filtered excitation and response signals with a 2-channel differential mode 16-bit ADC, and measure impedance using DFT.

In the final phase, different modules of hardware and software were tested individually, and results were documented. Potential error sources and enhancements were discussed.

This thesis is written in English and is 37 pages long, including 6 chapters, 24 figures and 4 tables.

## Annotatsioon

Selle lõputöö eesmärk on uurida ja arendada digitaalse signaaliprotsessori (DSP) põhise impedantsspektroskoopia süsteemi. Lõplik seade sisaldab oma funktsiooni teostamiseks analoogahelatega täiendatud elektroonikaplaati, mis põhineb kahetuimalisel TMS320F28379D mikrokontroller-DSP-l (Texas Instruments). Riist- ja tarkvara ühendamisega saab mitmekülgse, suhteliselt odava ja kohandatava impedantsi mõõtmise süsteemi, mida saab kasutada erinevates rakendustes.

Selle projekti alguses uuritakse erinevaid impedantsspektroskoopia meetodeid ja teostust. Pärast seda on loetletud vajalikud parameetrid ja arenduse eesmärgid. Seejärel on valitud trükkplaadi loomiseks lisakomponendid. Kuna eeldatakse, et impedantsspektroskoopiaseade analüüsib objekti vahelduvvoolu reaktsiooni, tuleb lisaks kõrgsageduslikule müra filtreerimisega eemaldada ka alalisvoolusignaali. Skeemi simuleeriti iteratiivselt ja arendati täpseks mõõtmiseks. Trükkplaat töötati välja kahe erineva operatsiooni-võimendi komplekti jaoks ja monteeriti kokku.

Seejärel teostati tarkvara arendus tööülesande põhjal. Siinus- ja koosinus korrelatsiooniga impedantsi mõõtmiseks kasutatakse kõrge eraldusvõimega impulss-laiusega binaarse ergastussignaali genereerimist, kasutades 2-kanalilist diferentsiaalrežiimil 16-bitist analoog-digitaalmuundurit.

Lõppfaasis testiti riist- ja tarkvara erinevaid mooduseid eraldi ning tulemused dokumenteeriti. Lõpuks käsitletakse võimalikke vigade põhjuseid ja võimalikke täiustusi. See lõputöö on kirjutatud inglise keeles ja see sisaldab 37 lehekülge, 24 joonist 4 tabelit.

## List of abbreviations and terms

ADC	analog to digital converter
DFT	discrete Fourier transform
DIP	dual in-line package
DSP	digital signal processor
GPIB	general purpose interface bus
HR-PWM	high resolution pulse width modulator
IC	integrated circuit
MSPS	million samples per second
Op-amp	operational amplifier
OUT	object under test
PC	personal computer
PCB	printed circuit board
PWM	pulse width modulator
SCI	serial communication interface
SMD	surface-mount device
SOIC	small outline integrated circuit
VCC	voltage common collector
V <sub>pp</sub>	voltage peak-to-peak

## Table of contents

1	Introduction .....	11
1.1	Background, definitions, and history .....	11
1.2	Overview of the thesis .....	12
2	State-of-the-art.....	13
2.1	Problem.....	13
2.2	Purpose.....	14
2.3	Applications .....	15
2.4	Similar devices.....	15
3	Overview of the components.....	17
3.1	Hardware.....	17
3.1.1	TMS320F28379D.....	18
3.1.2	PCB add-on .....	19
3.2	Software .....	20
3.3	Selection of components .....	21
3.4	Cost analysis .....	22
4	Theory, design, and solution .....	24
4.1	Mathematical background and simulations .....	24
4.1.1	Cross-correlation .....	24
4.1.2	Excitation signal .....	27
4.2	Circuit description.....	28
4.2.1	Filters .....	29
4.2.2	Virtual ground .....	32
4.3	PCB design .....	33
4.4	ADC, PWM and other peripherals.....	34
5	Tests and results .....	38
5.1	Excitation filters.....	39
5.2	Response filters and inverters .....	41

5.3	Virtual ground.....	42
5.4	ADC and SCI.....	45
5.5	Future work.....	46
6	Summary.....	47
	References .....	48
	Appendix 1 – Non-exclusive licence for reproduction and publication of a graduation thesis .....	51
	Appendix 2 – PCB schematic.....	52
	Appendix 3 – Final prototype.....	53



## List of figures

Figure 1. Hardware block diagram .....	17
Figure 2. Pseudo-code .....	21
Figure 3. Cross-correlation .....	25
Figure 4. Cross-correlation with series resistor .....	26
Figure 5. Voltage divider.....	27
Figure 6. Spectrum analysis of binary excitation signal.....	28
Figure 7. Circuit diagram – LTSpice.....	29
Figure 8. Second order active low-pass filter [10] .....	30
Figure 9. Active low-pass filter simulation .....	31
Figure 10. Virtual ground circuit.....	32
Figure 11. PCB layout: (a) top layer, (b) bottom layer.....	34
Figure 12. Configuring 16-bit differential ADC .....	35
Figure 13. HR-PWM configuration.....	36
Figure 14. Integer converter .....	37
Figure 15. Assembled PCB after modifications .....	38
Figure 16. 10kHz input signal test with oscilloscope.....	39
Figure 17. 100kHz input signal test with oscilloscope.....	40
Figure 18. 100kHz input signal test with simulation.....	40
Figure 19. Corner frequency measurement of excitation signal by simulation.....	41
Figure 20. Filtered response signal waveforms for differential ADC inputs, oscilloscope result. ....	42
Figure 21. Filtered response signal waveforms for differential ADC inputs, simulation measurement.....	42
Figure 22. Virtual ground voltage variation at 10 MHz input signal for OP2350 .....	44
Figure 23. Virtual ground voltage variation at 10 MHz input signal for MCP6022-I/A .....	44
Figure 24. ADC SCI test .....	45

## **List of tables**

Table 1. TMS320F28379D Features .....	18
Table 2. Main features of OPAX350 and MCP6022-I/P .....	20
Table 3. Cost table .....	22
Table 4. Virtual ground test for different frequencies .....	43

# 1 Introduction

## 1.1 Background, definitions, and history

Electrical impedance is usually defined as an expression of opposition of a circuit to alternating current. The term impedance is brought to the literature by Olivier Heaviside in 1886 [1]. Impedance is a complex quantity whereas resistance forms the real part and reactance makes the imaginary part [2]. Impedance is usually expressed in cartesian coordinate system as  $R+jX$  or in polar coordinate system as  $|Z|$  and  $\theta$  whereas  $|Z|$  represents magnitude and  $\theta$  represents angle of this complex quantity.

Impedance spectroscopy is measurement and analysis of impedance related variables and plotting of these variables in a complex plane [2]. There are different methods to measure and calculate impedance of an unknown object, such as AC bridges, phase-sensitive detectors, direct measurement with oscilloscope, automated frequency response analysis and using DSP (digital signal processor) [2].

Proposed impedance spectroscopy solution based on DSP method. In general, this kind of impedance spectroscopy devices usually consist of signal generator, current sensor, ADC (analog to digital converter) and DSP engine to process DFT (discrete Fourier transform). There are chip solutions based on this idea and Analog Devices AD5933 IC [4] can be given as an example.

Other type of devices to measure impedance is lock-in-amplifier type such as Zurich Instruments MF-IA which is phase sensitive detector. Although the latest one offers superior precision and wide frequency range, with the development of digital signal processing in parallel with lower power consumption open new possibility to develop more adaptable, mobile, cheaper impedance spectroscopy devices. Impedance spectroscopy can now be used for more than just laboratory purposes thanks to these new capabilities.

## 1.2 Overview of the thesis

The development and experimental setup of the Texas Instrument LAUNCHXL-F28379D [3] DSP development board-based impedance spectroscopy device are described in this thesis work, which includes features such as external active low pass filters, virtual ground approach for DC voltage elimination, binary, multifrequency excitation signal, and 16-bit differential ADC configuration.

In the next section general information about impedance spectroscopy devices, problems and purposes of different methods is given. After that, under more specific scope the uniqueness of the system handled in this thesis work are discussed. Furthermore, similar devices and application areas are investigated.

In the following chapter, brief descriptions about the hardware and software components used in this thesis work are discussed along with tables and block diagrams to provide a general impression about the final design. In addition, the same chapter discusses component selection rationale and cost analysis.

In the following section, actual design and implementation supported by theory is described. Along with simulation findings from the LTSpice and Matlab programs, comprehensive information about hardware and device design preferences is given here. As a part of this thesis work, analog circuit is designed and implemented as a PCB (printed circuit board) add-on for DSP utilizing Eagle PCB design program. Overcoming design challenges are seen in this section. Software of the system is written via Code Composer Studio [17] integrated development environment and some of the most important aspects of software is reviewed here.

Subsequently, the final device is put to the test in a variety of ways, and the effects are addressed. To better reveal flaws, the system subblocks tested individually using oscilloscope and signal generator. Obtained results are compared with simulation findings and error sources are revealed.

In the final chapter, summary of this thesis work is given along with possible enhancements discussion. Finally, a reference list and an appendix with additional figures are included.

## 2 State-of-the-art

This section discusses impedance spectroscopy devices' problems, solutions, various applications, and related devices.

### 2.1 Problem

Many sensors in molecular biology, electrochemistry and other fields represent changes in physical parameters in impedance amplitude and phase. The voltage/current relationship must be calculated with a minimum level of ambiguity in order to correctly calculate the impedance.

Impedance spectroscopy instruments range from low-cost chip-based solutions to high-end network analysers, each with its own set of benefits and drawbacks. For example, the AD5933 IC [4] offers a simple solution for measuring impedance, but it is limited to only one excitation frequency under 100 kHz, and many applications need more than one frequency to evaluate a model with more than two elements [5]. Network analysers, or lock-in-amplifiers, on the other hand, have a wide range of applications but are not ideal for certain cases due to their large size and high cost.

Between the two other approaches described previously, there is a need to build more adaptable, mobile, and less expensive devices. It is now possible to meet these criteria thanks to recent advancements in digital signal processors[6] which requires signal conditioning, analog to digital converting and running signal processing algorithms [6].

DSP-based designs, on the other hand, face challenges such as filtering high-frequency noise in the excitation signal, DC level shifting, and ADC sampling precision. These difficulties can be solved by using external active filters, creating virtual ground, and using the TMS320F28379D board's high resolution PWM and 16-bit differential ADC inputs. This study focuses on the issues that arose during the development of the DSP-based impedance spectrometry device.

## 2.2 Purpose

This thesis aims to investigate the possibilities of development of low-cost, portable, power-efficient impedance spectroscopy system based on a TMS320F28379D DSP board with an external PCB add-on. DSP should produce a multi-frequency excitation signal, sample filtered excitation and response signals, run a signal processing algorithm to measure the object's impedance, and communicate with the PC (personal computer) in real time. Low-pass filters must be used on the designed PCB to remove high-frequency harmonics of the excitation signal as well as external noise. A virtual ground circuit is also included on the PCB to remove the DC portion of the input signal and to act as a reference for inverters to prepare the signal for differential ADC. Furthermore, when operating within the limits of op-amps (operational amplifier), the PCB can scale signals to optimize ADC dynamic range. The list below contains more extensive details about the intended purpose.

- Except for displaying measurement result, the device must be self-sufficient.
- Over 100 kHz multifrequency excitation signal should be produced by the unit.
- Maximum excitation voltage – 3.3 V
- For excitation and response signals, the system should have two differential 16 bit ADC channels running at the same time.
- Low-pass filters should be included in the system.
- The excitation signal's DC content should be removed by the device.
- The device should calculate the result and send it to the PC in real time through serial communication.
- Changeable reference resistor to match with measured impedance for higher accuracy.
- Overall cost of the product should be under 100 euro.

## 2.3 Applications

Impedance spectrometry has many applications including medicine, biology, chemistry and more [8]. Bioimpedance has become increasingly relevant in medicine as a diagnostic and monitoring method. Combining bioimpedance measurement with other observable bioelectrical signals like electrogastrogram are used to detect the gastric muscle to detect shrinkage of gastric muscle [9]. A 16-bit A/D converter was used for electrogastrogram and a 24-bit A/D converter was used to calculate impedance using four contacts in this solution. Impedance was measured with a 2mA excitation current at a fixed frequency of 50kHz for this application.

Impedance measurements are also used in cell and molecular biology to describe a molecule's binding to specific macromolecules. System-on-chip devices that calculate impedance with attofarad resolution are available for use in antibodies, receptors, and DNA research at the nanoscale stage [10]. To prevent harming biological specimens, the system only applies a few tens of millivolts to them.

Soil content analysis is another application for impedance spectroscopy instruments. A documented method [11] for analysing sulphate saline soil to determine sulphate concentration and water content in the soil is an example of geotechnical application. The system's impedance response in the range of 0.1 to 100 kHz is investigated in this non-destructive and real-time measurement.

## 2.4 Similar devices

One of the most similar devices is developed by Estonian company Eliko. Its Quadra Impedance Spectroscopy [12] device allows for real-time measurements to be taken on the go. Thanks to a multifrequency binary excitation signal, this system may acquire impedance data in 15 different frequencies in 1 ms. The highest frequency set, which spans up to 349 KHz and is suitable for biological and material science measurements, is available. The lowest set of frequencies is optimal for electrochemical applications and ranges from 0.5 Hz to 195 Hz. Within the excitation signal range of 0.2 Vpp to 3.8 Vpp, measurement repeatability of 0.1 percent is promised. The device is operated by a USB connection, and the measurement results are sent to the machine by the same connection. The cost is 2.100 euros, according to the company's website.

Sciensoria, a French company that specializes in non-destructive research and instrumentation, offers one of the most straightforward strategic solutions. Their Z-Scope v6 measuring system [13] is used to measure conductive material thickness, electrical conductivity, displacement, and other parameters. The device's sinusoidal excitation frequency ranges from 100 Hz to 100 kHz, and it has two inputs for measuring input and output signals, much like ours.

Another Wayne Kerr Electronics solution is a precision impedance analyser [14] that can measure up to 120 MHz. The company's 6500B series guarantees 0.05 percent simple measurement precision. Its AC drive level varies from 10mV to 1V rms depending on frequency. This impedance analyser has a built-in colour monitor and can determine series and parallel circuits. The equivalent circuit analysis function can differentiate between four different types of three and four-component models. Besides that, it is possible to programme this device over GPIB (general purpose interface bus) or LAN. Overall, this instrument provides accurate and systematic measurements at higher frequencies.

Taking into account the devices and methods presented in this section, this thesis proposes a professional, robust, relatively inexpensive, and scalable impedance measurement system that can be used in a variety of applications.



### 3 Overview of the components

Brief explanations of the hardware and software components used in this thesis work, as well as tables and block diagrams, are discussed in this chapter to give a general understanding of the final design. Subsequently the reasoning for component selection and cost analysis are also discussed in this chapter.

#### 3.1 Hardware

In Figure 1 below, you can see overall hardware elements and their connections.

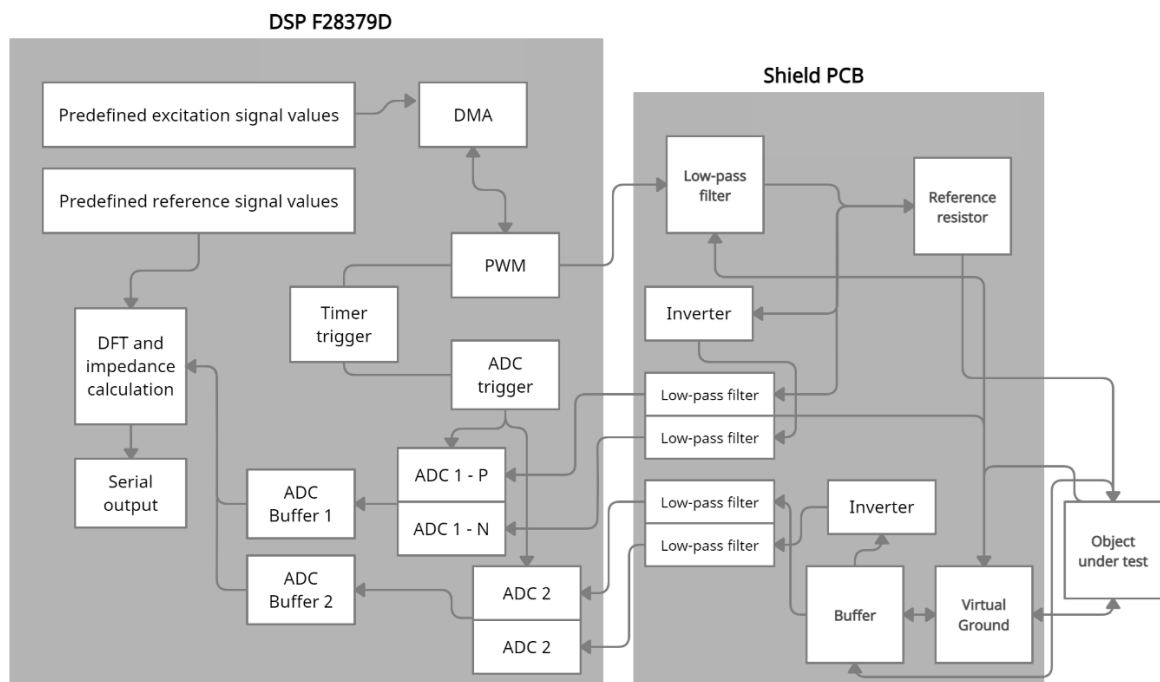


Figure 1. Hardware block diagram

As you can see from this block diagram, hardware is grouped in two groups, namely DSP F28379D and shield PCB. Second-order active low-pass filters are used on the PCB, and one of the two Op-amps, Texas Instruments' OPA2350 or Microchips' MCP6022-I/P, can be used. The same Op-amps are also used for buffer, virtual ground and inverter elements.

Main features of used DSP namely Texas Instruments TMS320F28379D Dual-Core Microcontroller is given in the following subsection.

### 3.1.1 TMS320F28379D

TMS320F28379D [3] is a member of Texas Instruments' C2000 32-bit microcontroller series, which is designed for real-time computation, sensing, and actuation in a wide variety of applications, including automotive motor drivers, transportation, sensing, signal processing, and more. It is a dual-core microcontroller that enables multitasking and eliminates the need for multiple processors in some applications. It is capable of performing signal processing tasks at 200 MHz. Furthermore, the system includes 24 improved pulse width modulator (PWM) channels. Also, its differential ADC subsystem is capable of performing high, low and zero crossing compare, saturating offset calibration and more. Core of the device is operated on 1.2V level while its I/O ports operates on 3.3V. Table 1 provides additional technical information [3].

**Table 1. TMS320F28379D Features**

<b>Processor</b>	
Number of CPU	2
Frequency (MHz)	200
DMA	Yes
Floating-point unit	Yes
<b>Memory</b>	
Flash	1MB
RAM	204KB
<b>System</b>	
Configurable logic block	Yes
32-bit CPU timers	6
Watchdog timers	2
I/O pins (GPIO)	97
External interrupts	5

**Table 2. TMS320F28379D Features**

<b>Analog peripherals</b>		
16-bit ADC	MSPS	1.1
	Conversion time	915 ns
	Input pins	20
	Differential channels	9
12-bit ADC	MSPS	3.5
	Conversion time	280 ns
	Input pins	20
	Differential channels	9
Number of ADCs		4
<b>Communication Peripherals</b>		
CAN		2
I2C		2
SCI		4
SPI		3
USB		1

The device will be powered by a USB cable that will also be used for serial communication with the computer. Above DSP device custom made PCB board will be placed. More information about PCB add-on is given in the next subsection.

### **3.1.2 PCB add-on**

PCB add-on is designed to complement the operations of DSP. It consists low-pass filters, virtual ground section, voltage regulator and connector to connect reference resistor and the object to be tested. This PCB was created using EAGLE software and was produced using online services. Its dimensions are 86.4 mm x 58.4 mm, and it was created to fit on a DSP unit. The circuit involves 6 op-amps. Two different high speed and dual packed op-amps were chosen to be tested and compared in this circuit. Because of the device's 8-pin dip sockets, it can be used with any set of interchangeable op-amps in the final edition. In the Table 3 below, you can see main features of chosen op-amps, Texas Instruments' OPA2350 [15] and Microchips' MCP6022-I/P [16].

**Table 3. Main features of OPAX350 and MCP6022-I/P**

	<b>OPAX350</b>	<b>MCP6022-I/P</b>
Rail-to-rail input	Yes	Yes
Wide bandwidth	38 MHz	10 MHz
Low noise	5 nV/ $\sqrt{\text{Hz}}$	8.7 nV/ $\sqrt{\text{Hz}}$
Total harmonic distortion	0.00060 %	0.00053 %
Unity-gain stable	Yes	Yes
Supply voltage range	2.5 V – 7.0 V	2.5 V – 5.5 V
Dual packaging	Yes	Yes

Both op-amps are intended to be used in different applications including audio processing, data acquisition, active filters and test equipment. Each of these parts can be powered by a single power source. Note that, there is not 8 pin dip packet available for OPA2350. To solve this issue, I ordered SOIC (small outline integrated circuit) to DIP (dual in-line package) adapter to be able to interchange op-amps in final device. Beside these active components, 3.3V regulator, SMD (surface-mount device) resistors, SMD and through hole capacitors, connectors and jumpers. More information about these components can be acquired from cost analysis section.

### **3.2 Software**

Software of the project is written by using Code Composer Studio 10.1.1 IDE by Texas Instrument [17]. This integrated development environment is based on Eclipse software framework and integrates embedded-debug capabilities. It supports different microcontroller and processor families from TI, including C2000 series [18]. Based on example codes and built-in functions, software of this project is written in C/C++ language.

Figure 2 below explains pseude-code of the software.

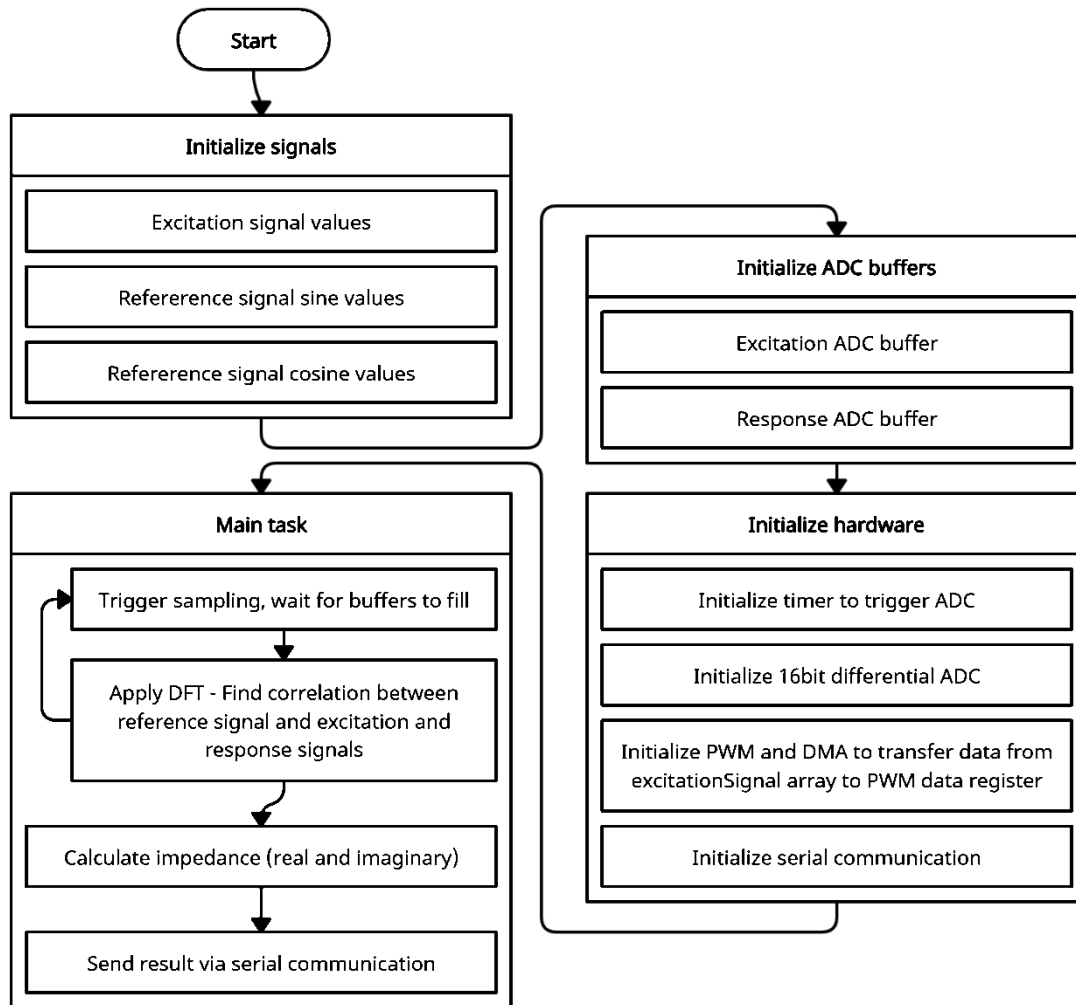


Figure 2. Pseudo-code

Note that, this approach can be expanded for more than one frequency by defining several reference signals and applying sine correlation for each frequency. Detailed software analysis is provided in following chapter.

### 3.3 Selection of components

The PCB design and external component selection for this project were focused on design specifications such as frequency range, accuracy, and cost. Six op-amps are used in the designed analog circuit. Two separate op-amps were chosen in the final version to test and compare performance. Dual packed op-amps were chosen to make routing simpler. One of the main requirements from these active components is wide bandwidth. Both the OPAx350 and the MCP6022-I/P are high-speed op-amps with 38 MHz and 10 MHz

bandwidths, respectively. Since measurement accuracy is important for this project, low-noise levels were also considered. Another limiting factor was voltage supply range. In designed circuit we can provide 3.3 V or 5 V single power supply and both devices are able to operate in this range. Later in this thesis, trade-of between two selected op-amps are discussed.

As of passive components, size, and tolerance values along with low ESR values for capacitors were considered. All resistors on the PCB are 0805 type and soldered except reference resistor which is high precision resistor and can be connected through screw terminal block. The packaging type of components were chosen to be small enough to fit on the PCB and big enough for manual soldering. Ceramic disk capacitors are used as coupling capacitors due to their very low ESR values [19]. Having both SMD and through hole components simplified routing for 2-layer PCB.

### 3.4 Cost analysis

Most of the components of the system including DSP were ordered from Farnell website. PCB itself and box are exemptions. Table 4 below shows the components and their costs.

**Table 4. Cost table**

Component	Farnell order code	Quantity	Price per unit – Euro (excl. VAT)	Total price – Euro (excl. VAT)
SMD Capacitor 10uF	1657936	3	0.605	1.815
SMD Capacitor 100p	7568665	2	0.195	0.39
SMD Resistor 5kOhm	2616759	3	0.134	0.402
SMD Resistor 10kOhm	2078962	7	0.017	0.119
SMD Resistor 10Ohm	2333619	4	0.0164	0.0656
SMD Resistor 100kOhm	1160261	1	0.415	0.415
SMD Resistor 50kOhm	1857226	1	2.15	2.15
SMD Resistor 1kOhm	2078907	1	0.0446	0.0446
Ceramic capacitor 30p	2819662	1	0.751	0.751
Ceramic capacitor 33p	1141761	4	0.275	1.1
Ceramic capacitor 5p	2860017	2	1.18	2.36
Ceramic capacitor 0.1uF	2859995	5	0.15	0.75

<b>Component</b>	<b>Farnell order code</b>	<b>Quantity</b>	<b>Price per unit – Euro (excl. VAT)</b>	<b>Total price – Euro (excl. VAT)</b>
Voltage regulator 3V3 LE33CZ	3130064	1	0.765	0.765
Dual OpAmp OPA2350	3117462	3	5.4	16.2
SOIC8 to DIP8 adapter	2476033	3	3.12	9.36
DIP8 socket	2668408	3	0.152	0.456
PCP receptable	2667433	4	1.31	5.24
Terminal block 2 ways with screws	2668641	2	0.488	0.976
Dual OpAmp MCP6022-I/P	9758640	3	1.32	3.96
Jumper 2 way	2112496	1	0.251	0.251
Pin header	2751452	1	0.227	0.227
TMS320F28379D	3126117	1	34.39	34.39
PCB	xxx	1	0.4	0.4
Generic box	xxx	1	2	2
<b><i>Total price</i></b>				85

Shipping costs are not included because shipping costs per unit for one unit and multiple units will vary drastically. Furthermore, unlike the table above, only one set of op-amps will be included in the final design, so this table reflects prototyping costs rather than real unit costs.

As a result, the total budget of this project remains below the 100 euro target. The next section describes the device's implementation using the selected hardware and software components described in this section.

## **4 Theory, design, and solution**

This section describes the actual design and implementation, which is accompanied by theory. Different aspects of the applications are explored here, along with simulation results from the LTSpice and Matlab programs.

### **4.1 Mathematical background and simulations**

The system built in this thesis functions similarly to a circuit analyser. Excitation output stimulates the object under test and two inputs measure input and output. To extract impedance information, the sinus correlation method is used. An analog pre-processing circuit with low-pass filters, inverters, a virtual ground generator, and buffers were placed between DSP and OUT (object under test). In this portion, I will go over the design and implementation of each component of the system in detail.

#### **4.1.1 Cross-correlation**

Cross-correlation provides information about the similarity between two sequences [20]. It is used to detect frequency content of the signal which enables fast, accurate measurements over a broad frequency range while suppressing noise and harmonics [21]. By correlating measured signal with reference signals, it is possible to obtain complex impedance information from the circuit. Graphical description of the idea is given in the Figure 3 below.



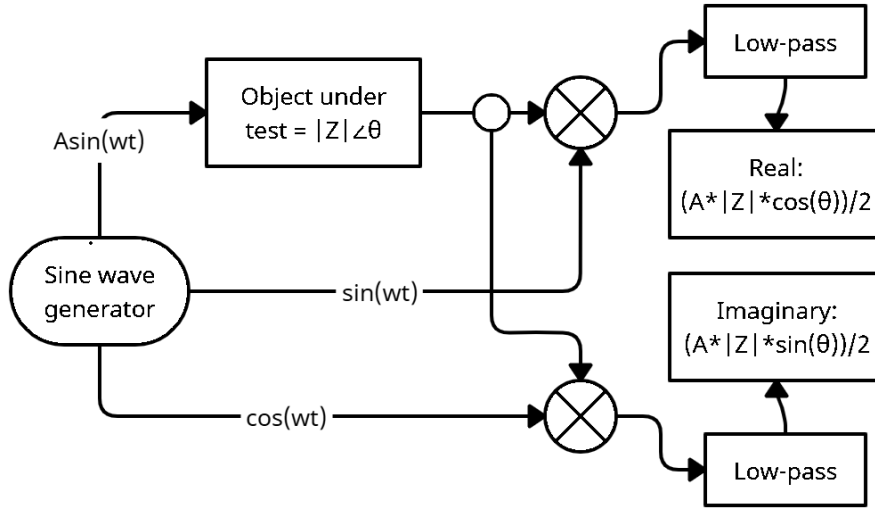


Figure 3. Cross-correlation

To prove this result mathematically we should start with sine multiplication equation (1) and equation (2).

$$\sin(a) \sin(b) = \frac{1}{2} (\cos(a - b) - \cos(a + b)) \quad (1)$$

$$\cos(a) \sin(b) = \frac{1}{2} (\sin(a + b) - \sin(a - b)) \quad (2)$$

Now assume object under test is complex number and it is expressed as  $|Z| \angle \theta$ . Now multiply generated sine wave to this value.

$$A \sin(\omega t) \cdot |Z| \angle \theta = A |Z| \sin(\omega t + \theta) \quad (3)$$

This output signal is then multiplied by reference signals. Correlation occurs at this stage. The results of applying equation (1) and equation (2) are as follows.

$$\sin(\omega t) \cdot A |Z| \sin(\omega t + \theta) = \frac{A |Z|}{2} (\cos(\theta) - \cos(2\omega t + \theta)) \quad (4)$$

$$\cos(\omega t) \cdot A |Z| \sin(\omega t + \theta) = \frac{A |Z|}{2} (\sin(2\omega t + \theta) - \sin(-\theta)) \quad (5)$$

At this step we have alternating (with twice of input frequency) and DC constant part of output signal. We can remove the alternating component of the equations (4 and 5) and obtain information about the real and imaginary parts of the object by using a low-pass filter (integrator).

$$\frac{1}{t} \int \frac{A|Z|}{2} (\cos(\theta) - \cos(2\omega t + \theta)) dt = \frac{A|Z|}{2} \cos(\theta) \quad (6)$$

$$\frac{1}{t} \int \frac{A|Z|}{2} (\sin(\theta) - \cos(2\omega t + \theta)) dt = \frac{A|Z|}{2} \sin(\theta) \quad (7)$$

By multiplying these results with  $2/A$  we obtain  $|Z|\cos(\theta)$  and  $|Z|\sin(\theta)$  which is real and imaginary parts of  $Z$  consequently. Besides that, we are also applying this method to analyse input signal after filtering. Notice that, complex value of the object represents impedance and input signal represents current. We know current information by measuring voltage over series reference resistor. Figure 4 below, illustrates extended version of previous figure, combining series reference resistor to find current and calculate unknown impedance.

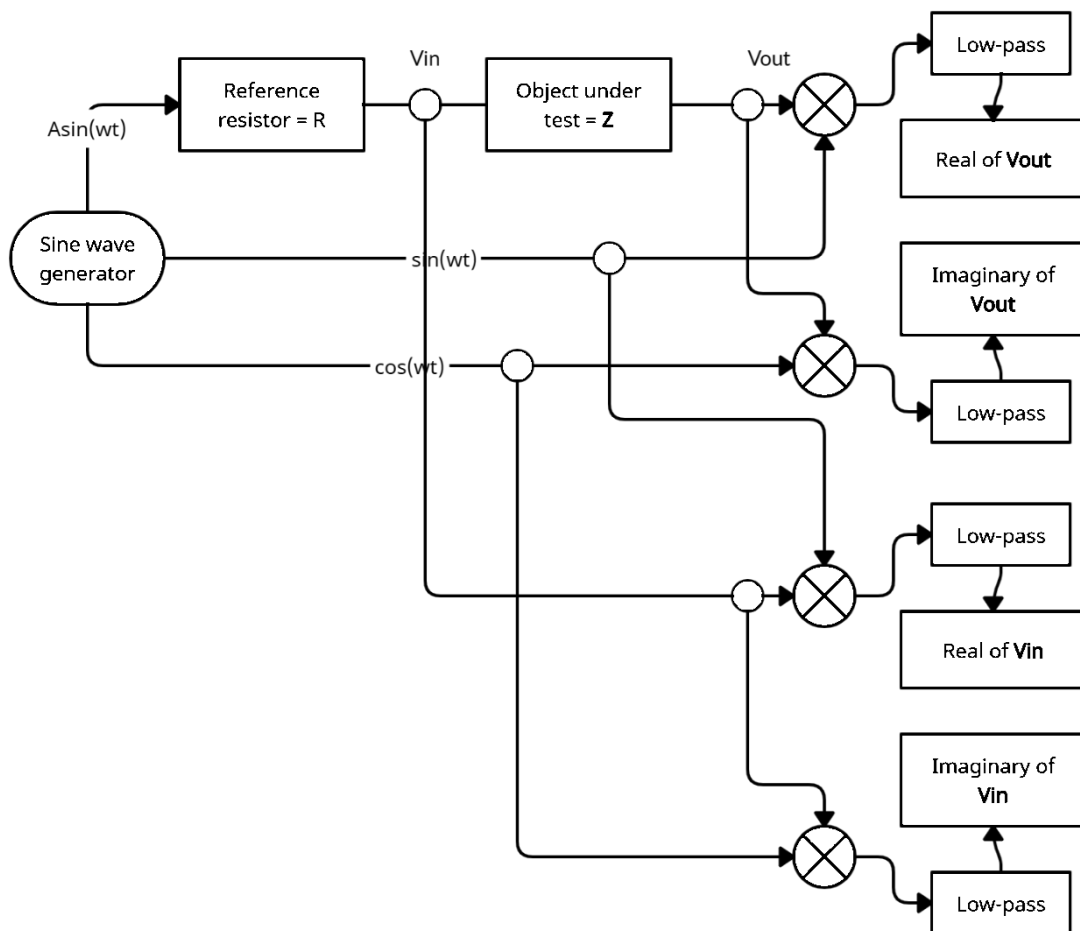


Figure 4. Cross-correlation with series resistor

As you can in this figure, cross-correlation analysis is applied at two points ( $V_{in}$  and  $V_{out}$ ) and we are able to find real and imaginary parts of the voltage signal at these points as

described above and hence amplitude and phase information. Now consider that series resistor and unknown impedances are connected in series as in Figure 5.

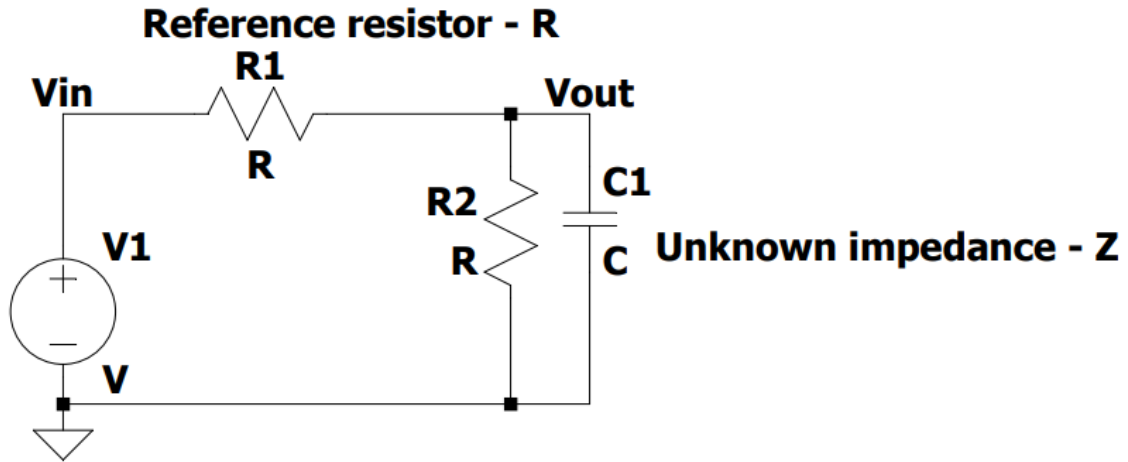


Figure 5. Voltage divider

Since we know amplitude and phase values at both points ( $V_{in}$  and  $V_{out}$ ) and reference resistor value, we can find amplitude of impedance from Ohm's law as below.

$$|Z| = \frac{|V_{out}|}{|V_{in}| - |V_{out}|} * R \quad (8)$$

And phase of the  $|Z|$  is simply differences of the phases at  $V_{in}$  and  $V_{out}$  as in Equation 9.

$$\angle Z = \angle V_{in} - \angle V_{out} \quad (9)$$

This method is applied with more than one frequency simultaneously to obtain spectral impedance information of unknown object.

#### 4.1.2 Excitation signal

Excitation signal generation is an important part of this design. Different excitation signals, such as single or multiple sine waves, chirp and binary signals can be used for excitation signals [22]. In contrast to sine waves, discrete waveforms may have a higher amount of useful excitation energy, according to [22]. Binary, multi-component excitation, according to the same source, has 76 percent or higher efficiency. Sinusoidal waveforms of desired frequencies are added in the continuous time domain to produce a binary excitation signal, which is then subjected to the signum operation [23]. I wrote a Matlab script to compare the frequency contents of multiple sine waves and a binary signal of the mentioned frequency set in [23], and you can see the results in Figure 6.

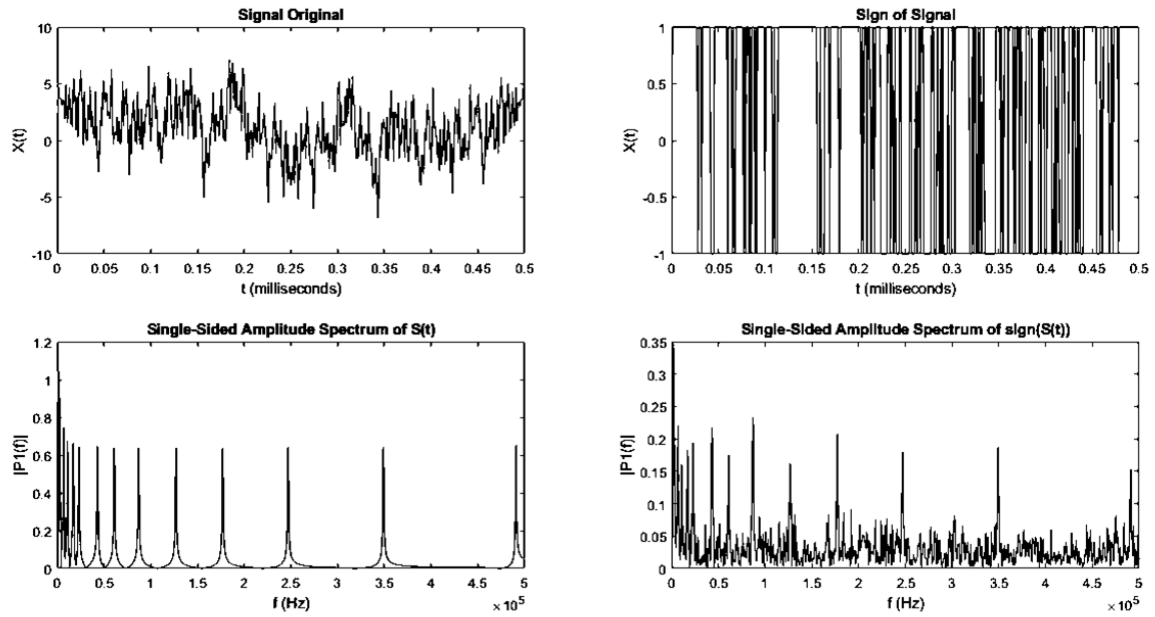


Figure 6. Spectrum analysis of binary excitation signal

As you can see, a binary signal with a strictly limited amplitude of  $\pm 1$  in time domain produces comparable spectrum results. Despite the fact that this approach introduces noise, binary signal has a higher energy density in desired frequencies and is simpler to produce, so it was chosen as the excitation signal.

## 4.2 Circuit description

Another important task is to design an electronic board supplemented with analog circuit to perform its function as PCB add-on. This circuit is simulated by LTSpice XVIII software. To simulate op-amps spice models are downloaded from manufacturer's website and added to the simulation. You can see constructed circuit diagram from the Figure 7.

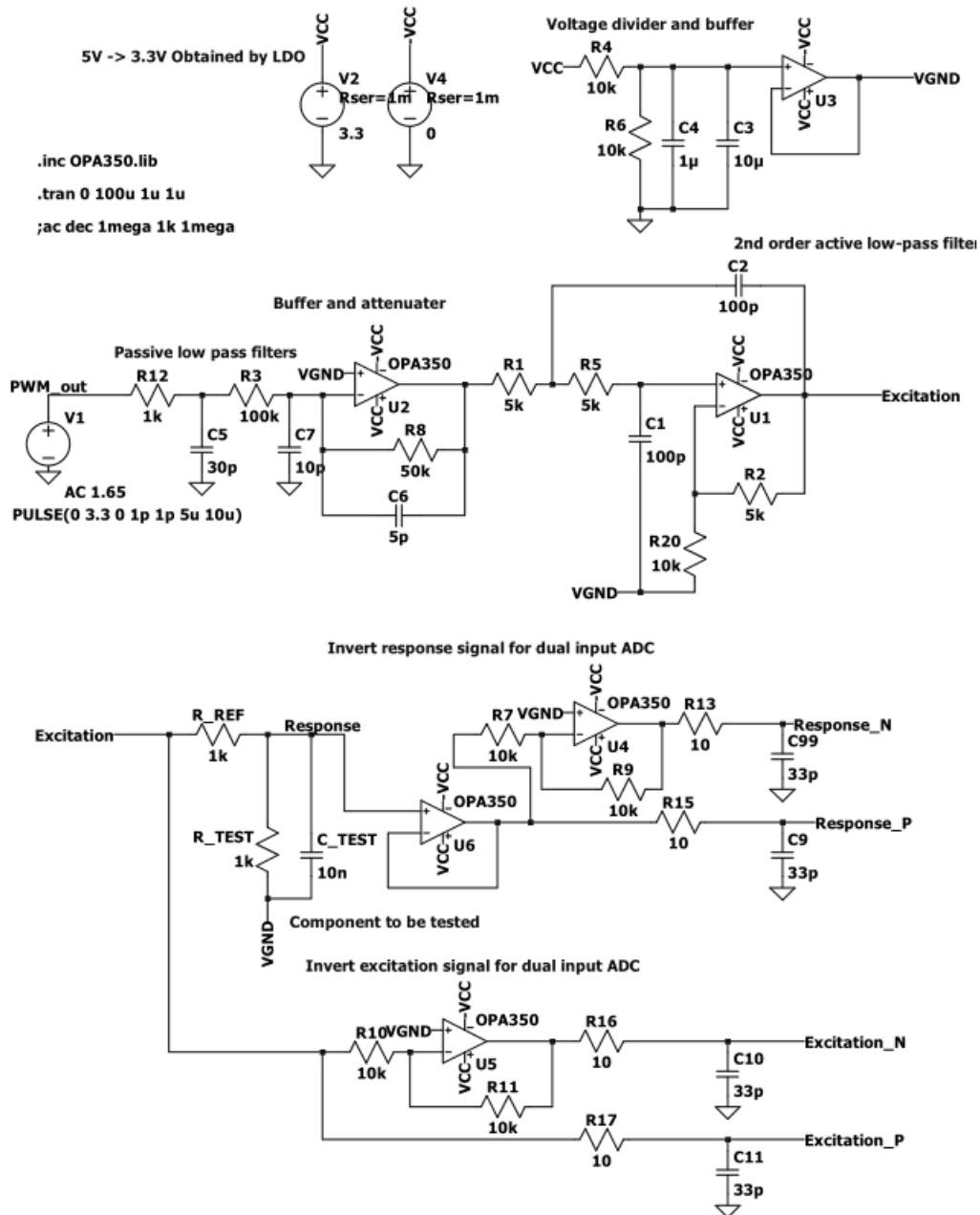


Figure 7. Circuit diagram – LTSpice

As you can see this circuit is capable of filtering PWM signal, generating virtual ground voltage level, and inverting excitation and response signal for differential mode ADC inputs. To increase readability, signal names – labels are used.

#### 4.2.1 Filters

Low pass filters are used to eliminate harmonics of PWM signal and high frequency noise. Between PWM output and buffer stage there is two first order low pass filters connected

in series. Calculating cut-off frequency from equation (10) below, first RC filter has approximately 5.3 MHz corner frequency.

$$f_c = \frac{1}{2\pi R C} \quad (10)$$

This frequency is higher than highest measurement frequency and its function is to eliminate spikes that PWM generator of DSP might introduce to the system between on and off states.

The next RC filter has 159.15 kHz corner frequency, and its function is to increase roll of rate and contribute to the second order active low-pass filter operation. Note that, resistor value is 100 kOhm is much higher than previous stage (1 kOhm), hence loading effect is negligible.

The first op-amp in this link acts as a buffer and attenuator. The input signal is attenuated by a factor of 2, because in the following stage resonance picking second order active low-pass filter is used and around this resonance frequency the output of the active filter could be clipped, particularly when supplied by 3.3 V level.

In the next stage second order active low pass filter is used and its isolated circuit can be seen from Figure 8 below.

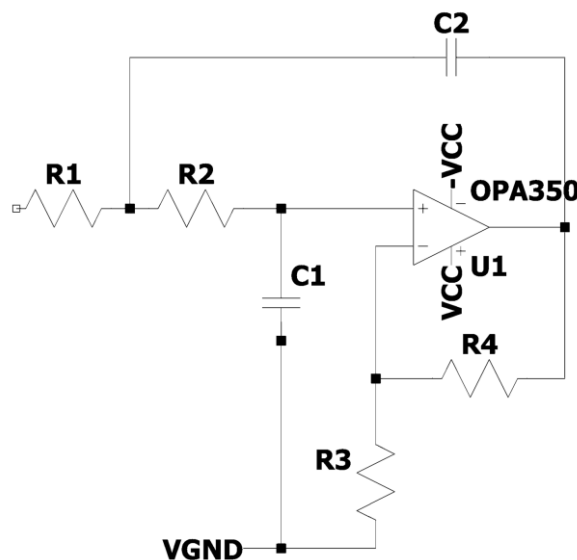


Figure 8. Second order active low-pass filter [10]

Transfer function of this second order active low pass filter is given in equation (11) below [10].

$$H(f) = \frac{\frac{R_3+R_4}{R_3}}{(j2\pi f)^2 R_1 R_2 C_1 C_2 + j2\pi f \left( R_1 C_1 + R_2 C_1 + R_1 C_2 \left( -\frac{R_4}{R_3} \right) \right) + 1} \quad (11)$$

This filter is also called Sallen-Key architecture [24] and to simplify this formula and proceed design, I selected  $R_1 = R_2$ , and  $C_1 = C_2$ . Since  $R_3$  and  $R_4$  only affects passband gain and quality factor, I have modified their values through simulation to obtain acceptable range. Consequently, corner frequency of this filter is dependent only from  $R_1, R_2, C_1, C_2$  and simplified equation (12) is as below.

$$f_c = \frac{1}{2\pi\sqrt{R_1 * R_2 * C_1 * C_2}} \quad (12)$$

After choosing capacitor values 100 pF, from equation (12), resistor values are calculated to equate cut-off frequency close to 250 kHz.

From the Figure 9 below, you can see simulation result of this filter.

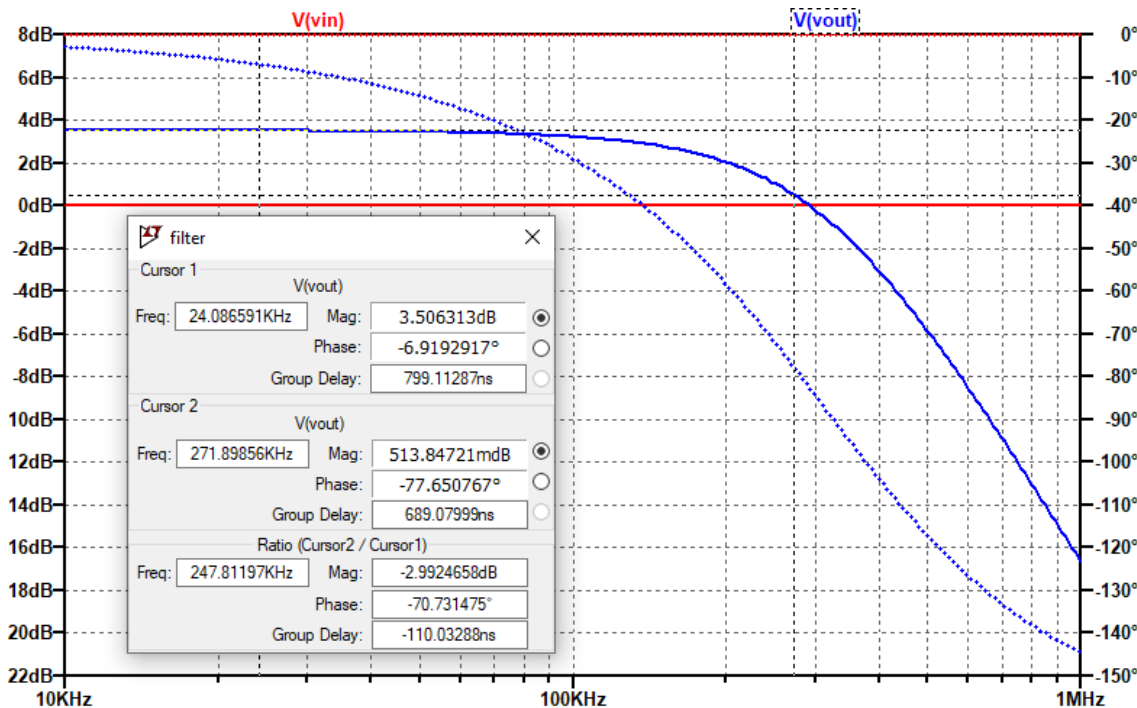


Figure 9. Active low-pass filter simulation

I performed AC analysis in the frequency range from 10 kHz to 1 MHz. From the cursor values 3dB attenuation of passband level occurs approximately at 271.89 kHz which is

compliant with our plan. Note that this filter is active and amplify its input by 3.5 dB while preserving flatness of pass-band region.

This second-order active filter subcircuit is also added to the response signal to filter external high-frequency noise from the tested component while also increasing the roll-rate for later ADC sampling. Since high-frequency noise can induce aliasing in sampling [25], I included this filter. Another RC filter is inserted right before the ADC inputs for the same reason.

Besides filtering these circuits have another function too. As you can see from Figure 9 above, C1 is connected to the virtual ground which allows us to shift the signal ground to the virtual ground level. More information about virtual ground is given in the following subsection.

#### 4.2.2 Virtual ground

We need to get rid of the DC part of the produced binary signal because this system is supposed to measure the object's resistance to alternating current. DC bias is a possible error source for impedance measurements, according to [5], despite the fact that DFT calculation eliminates it. Magnetic flux saturation caused by DC voltage, for example, will affect AC measurements for inductors. A virtual ground level is generated to solve this problem, and the simplified circuit used in this project can be seen in Figure 10 below.

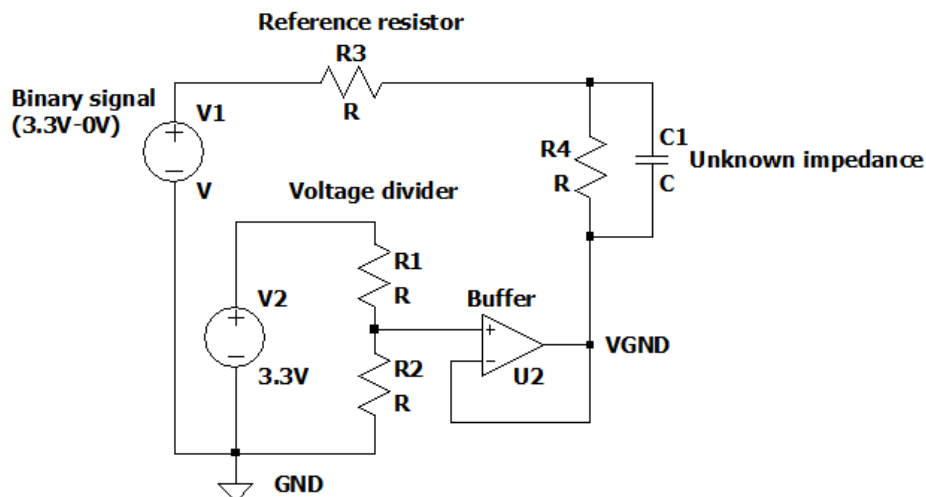


Figure 10. Virtual ground circuit



V1 represents a binary excitation signal, and its output is either 0V or 3.3V relative to ground in this circuit. V2 is a voltage source that produces a 3.3V DC. Half-voltage is supplied to the buffer input after the voltage divider portion with equal-valued resistors. Buffer is used to have low output impedance at virtual ground, which is 1.65V relative to the ground. Finally, the object under test is connected to virtual ground, eliminating the DC portion of the excitation signal for OUT.

Please note that there are some differences between this simplified diagram and the actual circuit, such as low-pass filters before the reference resistor and filtering capacitors at the positive input of the op-amp are added. Since the op-amp is not ideal in real life, its slow response to changes at the output and nonzero output impedance can cause issues, which is discussed in the next chapter.

### **4.3 PCB design**

PCB of the proposed device was designed with Eagle 9.6.2 software. The design was built on Booster Pack product provided by Element14 [26]. After deciding input and output pins of DSP to be used, the circuit was built as designed with LtSpice software. Full schematic of PCB can be seen from Appendix 2.

Before creating the PCB layout, I decided on the packaging types of passive components. SMD components with the packaging type 0805 are used for all resistors and some capacitors. Through-hole components include ceramic disk capacitors, voltage regulators, op-amp sockets and connectors. Two terminal blocks with screws have been added to make connecting the external reference resistor and OUT. DIP8 sockets have been introduced to make it easier to replace op-amps. These sockets are required because the OPA2350 op-amp does not have a DIP packet option, but it can be used in these sockets as an alternative to MCP6022-I/P op-amps using an SOIC8 to DIP8 adapter. Finished 2-layer PCB layouts can be seen from Figure 11 below.

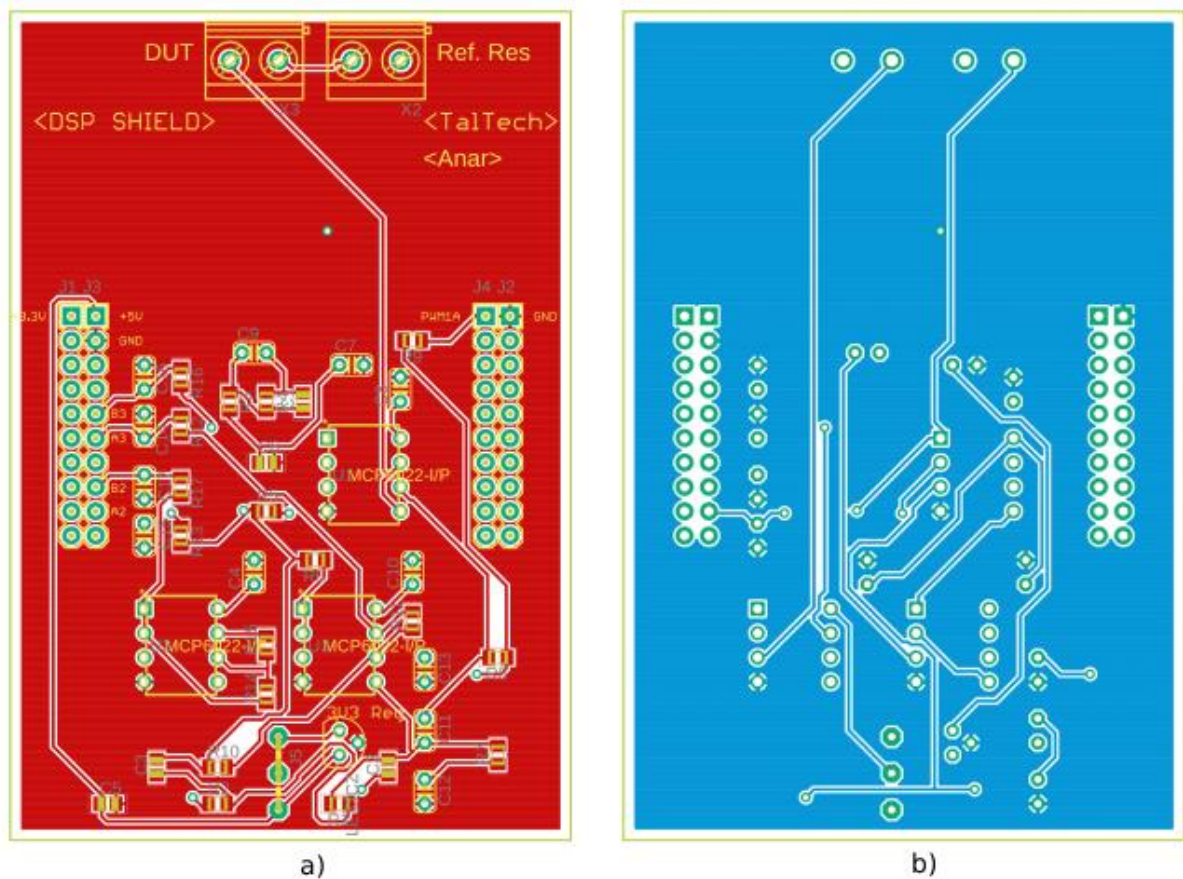


Figure 11. PCB layout: (a) top layer, (b) bottom layer

In addition to LtSpice circuit, decoupling capacitors are placed close to VCC (voltage common collector) pins of each op-amp and ground to provide stable voltage. Ground polygons are applied to both top and bottom layers to decrease distance between ground pins of the components and ground level and to provide very low impedance return path for power and high frequency signals. Overall size of this PCB is 58.4 mm x 86.4 mm, and it is manufactured through online service. Produced and assembled PCB can be observed in the next chapter.

#### 4.4 ADC, PWM and other peripherals

To accomplish tasks, on-board ADC, PWM, SCI and other peripherals should be configured with software. For data acquisition, 16-bit differential mode ADC converters within DSP module are used. According to the datasheet of TMS320F28739D [3], ADC hardware can be configured either in 12-bit mode or 16-bit mode. One of the main trade-off between these choices is conversion speed. In 16-bit configuration, 1.1 million samples per second (MSPS) can be achieved while, 12-bit configuration enables 3.5 MSPS

(million samples per second). On the other hand, 16-bit ADC is much precise than 12-bit mode and resolutions for 3.3 V full-scale voltage range is calculated using the equations (13 to 15) below [27].

$$Q = \frac{E_{FSR}}{2^M} \quad (13)$$

$$Q|_{E_{FSR}=3.3V, M=16} = \frac{3.3}{2^{16}} V \approx 0.00005V = 50\mu V \quad (14)$$

$$Q|_{E_{FSR}=3.3V, M=12} = \frac{3.3}{2^{12}} V \approx 0.00080V = 800\mu V \quad (15)$$

For the equations above, Q stands for resolution of ADC,  $E_{FSR}$  is full-scale voltage range [27] which is equal to 3.3 V for this project. While noise can influence the least significant bits of a 16-bit ADC, and measurement precision can be lower than shown here, 16-bit mode is still preferred. Aside from that, a 16-bit sampling rate of 1.1 MSPS is sufficient for our project, which does not require a sampling rate of more than 1MHz.

DSP's 16-bit ADC can only be configured with differential mode [3], which means two signals is supplied to the input pins and difference is measured. Inverting op-amps are used to generate differential signals from excitation and response signal for these inputs. According to [28], differential ADCs have many benefits, including rejection of common-mode noise in the microcontroller ground, doubling dynamic range, and the ability to directly hold negative values for negative part of the AC signal.

To configure 16-bit differential ADC to sample excitation and response signals, example codes from C2000Ware software [18] are used. From Figure 12. Configuring 16-bit differential ADC below, you can see some critical lines from the modified code.

```
// Set ADC to 16bit differential mode
ADC_setMode(adcBase, ADC_RESOLUTION_16BIT, ADC_MODE_DIFFERENTIAL);

//set ADC trigger source as ePWM2B
EPWM_setADCTriggerSource(EPWM2_BASE, EPWM_SOC_B, EPWM_SOC_TBCTR_U_CMPB);

// Set the compare B value to 25 and the period to 49
// Assuming ePWM clock is 100MHz, this would give 1MHz sampling
EPWM_setCounterCompareValue(EPWM2_BASE, EPWM_COUNTER_COMPARE_B, 25);
EPWM_setTimeBasePeriod(EPWM2_BASE, 49);

//Set ADC A2 and A3 to be differential channels
ADC_setupSOC(ADCA_BASE, ADC_SOC_NUMBER2, ADC_TRIGGER_EPWM2_SOCB,
```

Figure 12. Configuring 16-bit differential ADC

As you can see, A2 and A3 pins are used in differential configurations. Converted result can be read with ADC\_readResult() function. The same configuration is also done for B2 and B3 pins to sample the second signal.

Another peripheral that had to be configured was HR-PWM (high resolution pulse width modulator). HR-PWM can improve frequency spectra substantially by achieving more accurate zero crossing time when generating binarized multifrequency signals [23]. To test this peripheral, EPWM1A pin was programmed to 1MHz 50% duty-cycle output and critical parts of the code is given in the Figure 13 below.

```
// Set period
    initHRPWM(EPWM_TIMER_TBPRD);
    EPWM_setTimeBasePeriod(myEPWM1_BASE, period-1)

// Set duty 50% initially
    HRPWM_setCounterCompareValue(myEPWM1_BASE, HRPWM_COUNTER_COMPARE_A,
    (period/2 << 8));

// Set up counter mode to UP
    EPWM_setTimeBaseCounterMode(myEPWM1_BASE, EPWM_COUNTER_MODE_UP);

// Choose time based counter mode and prescale PWM clock
    EPWM_setTimeBaseCounterMode(myEPWM1_BASE, EPWM_COUNTER_MODE_UP);
    EPWM_setClockPrescaler(myEPWM1_BASE, EPWM_CLOCK_DIVIDER_1,
    EPWM_HSCLOCK_DIVIDER_1);

// MEP edge select
    HRPWM_setMEPEdgeSelect(myEPWM1_BASE, HRPWM_CHANNEL_A,
    HRPWM_MEP_CTRL_RISING_EDGE);
```

Figure 13. HR-PWM configuration

Besides excitation generation and response measurement, it is also necessary to send calculated results over serial link. In the given examples, SCI (serial communication interface) was set to send characters or strings and it is possible to use blocking or nonblocking serial connection in the given. Since the results we are getting (impedance and phase value) are expressed in decimal numbers, it is required to convert decimals to character array, and I wrote function given in Figure 14 below to perform this conversion and send data.

```

void writeInt (int val){
    char buffer [9];
    int temp;
    int i = 0;
    int length = 0;
    int negFlag = 0;
    if (val<0) { //consider negative numbers
        negFlag = 1;
        val = -val;}
    if (!val)//consider zero
        buffer[0] = 48;
    while (val){
        temp = val%10;
        val = val/10;
        buffer[i] = temp+48;
        i++;
        length++;}
    if (negFlag)
        SCI_writeCharBlockingFIFO(SCIA_BASE, 45); //negative sign
    while (length-->0)
        SCI_writeCharBlockingFIFO(SCIA_BASE, buffer[length]);
    SCI_writeCharBlockingFIFO(SCIA_BASE, 10); //newLine}

```

Figure 14. Integer converter

Different aspects of design and theory, such as mathematical perspective, simulations, PCB design, and software solutions, were discussed here. In the following chapter, experiments are carried out to test the suggested methods and results presented.

## 5 Tests and results

This section contains the outcomes of experiments that have been carried out. System modules are tested separately in order to validate the completed system. The subcircuits of the assembled PCB are reviewed before being attached to the DSP board. During the evaluation, it was discovered that certain errors were made during the layout design, which were investigated and corrected. The fully functional PCB after modifications is shown in Figure 15 below.

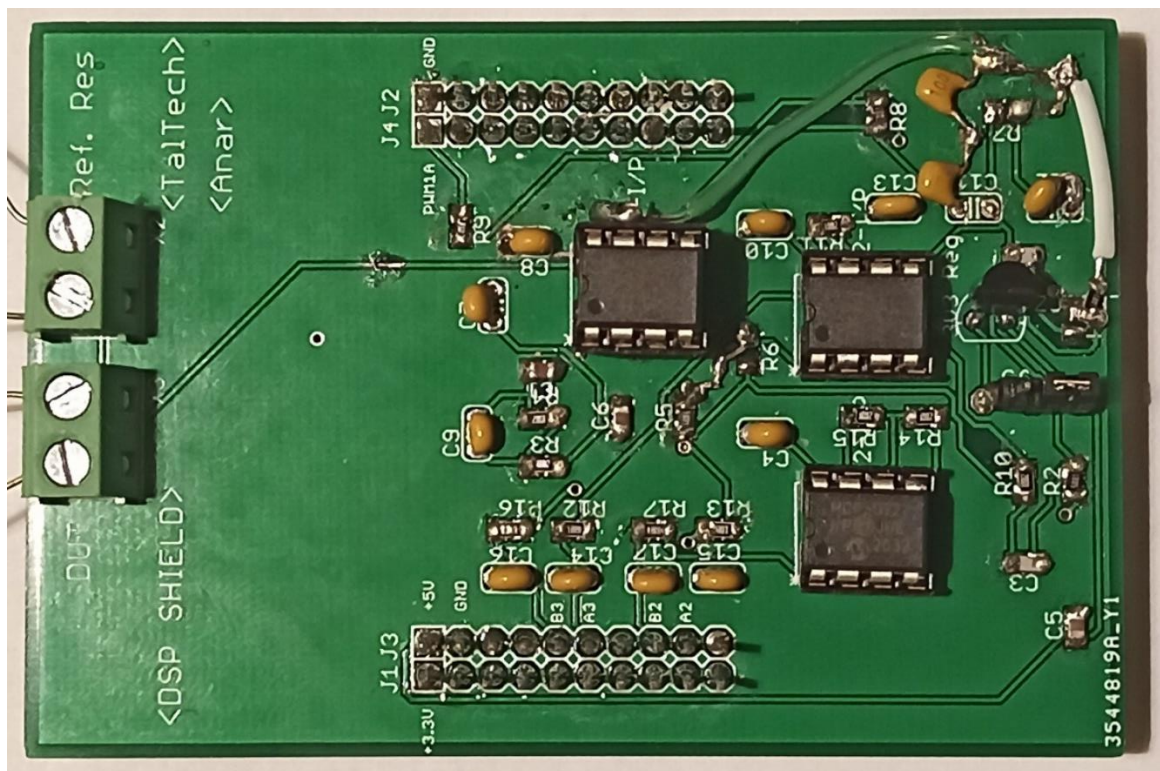


Figure 15. Assembled PCB after modifications

I tested PCB with oscilloscope – KEYSIGHT MSXOX2014A to correct faults.

## 5.1 Excitation filters

To be able to test low-pass filters, oscilloscope built in signal generator is used. From the Figure 16 below, you can see 10kHz, 50% duty cycle square wave input signal and filtered excitation signal.

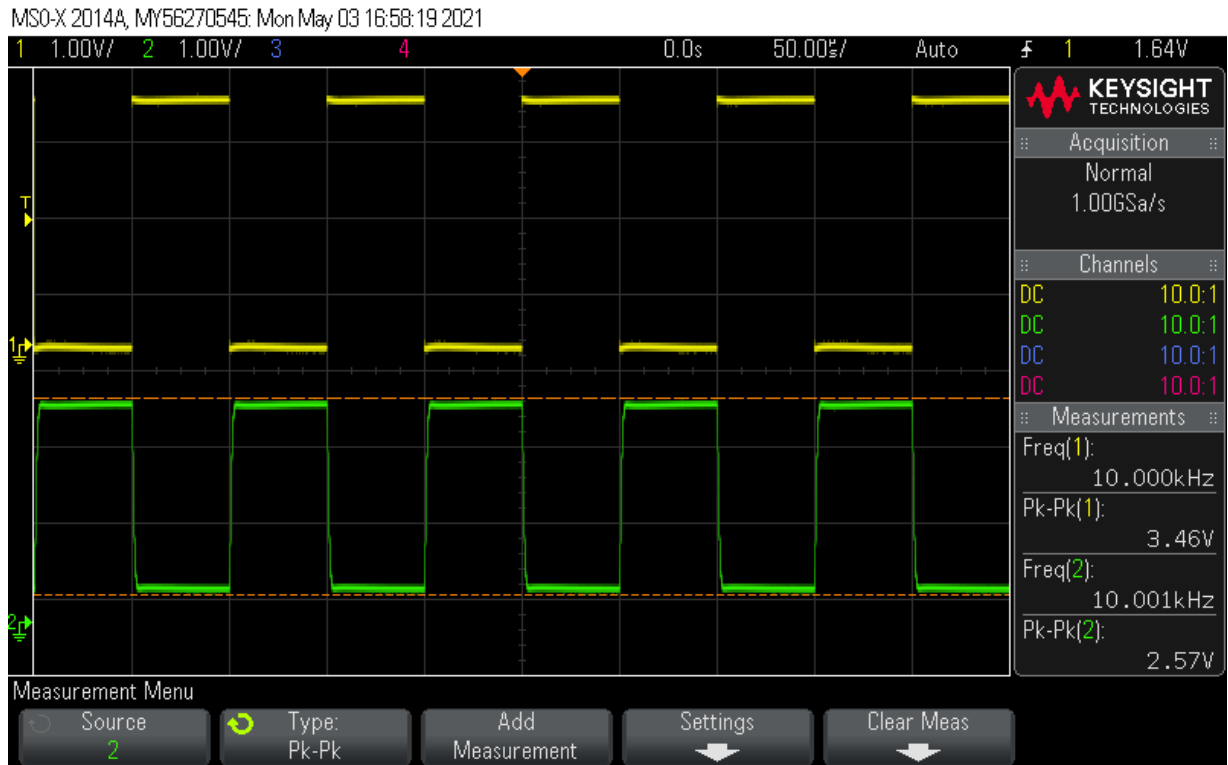


Figure 16. 10kHz input signal test with oscilloscope

Since, cut-off frequency of low pass filters is above 150 kHz, 10 kHz square wave input signal did not change much of its shape, except transition spikes filtered and DC level shifted. Although, peak to peak amplitude of built-in signal source was set to 3.3V, measurement shows 3.46 V due to overshoot. These overshoots are also expected from PWM generator of DSP, hence it is necessary to filter input signal.

Figure 17 shows waveforms from the same setup with 100kHz input signal.

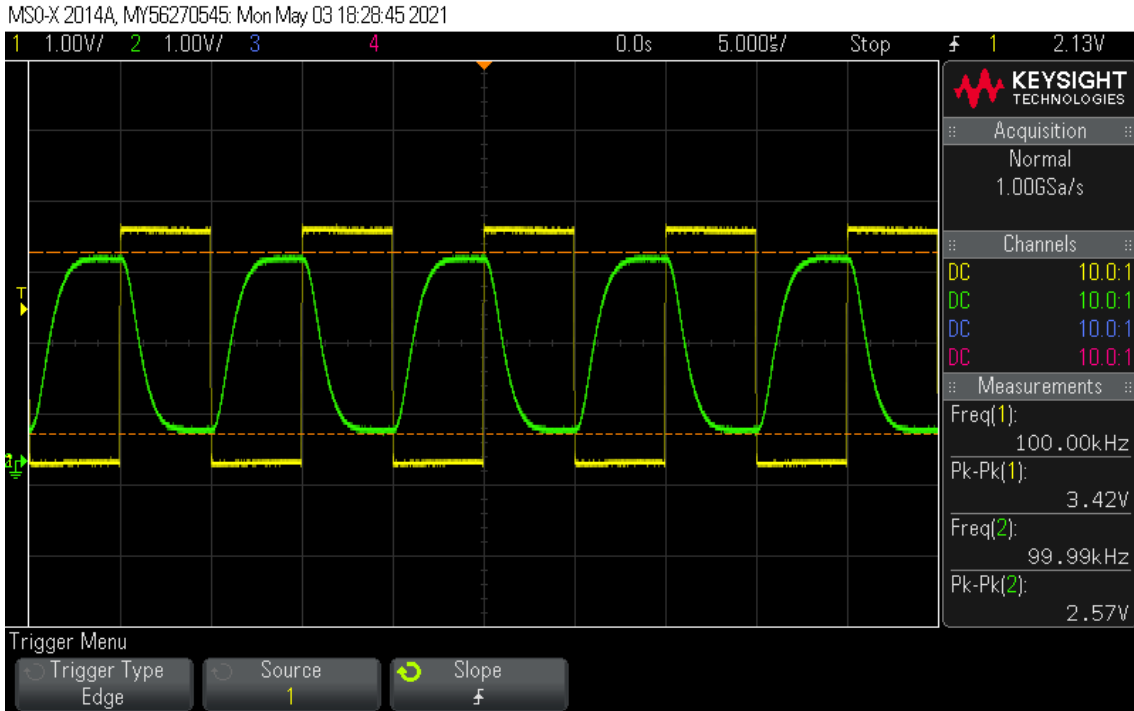


Figure 17. 100kHz input signal test with oscilloscope

As you can see, 100 kHz square signal more deformed due to loss of higher harmonics, but its peak-to-peak value is 2.57V which is same as 10 kHz signal. This fact shows that, low-pass filter has flat pass-band gain for this region. Figure 18 shows the same setup with LtSpice simulation to confirm operation of the PCB shield.

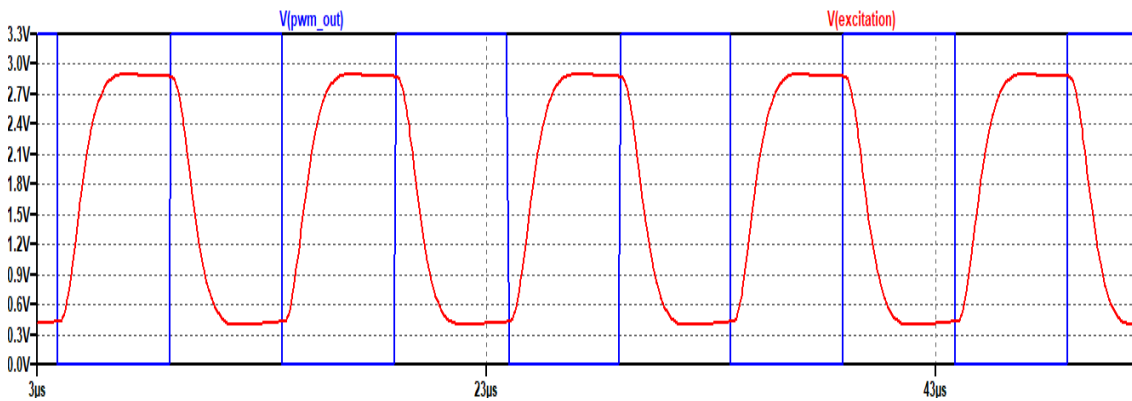


Figure 18. 100kHz input signal test with simulation

These figures also confirm the working of virtual ground. As you can see, filtered excitation signal is DC shifted and there is little margin between ground and 3.3 V level



left, which ensures proper operating of op-amps and ADC within their limits while maximizing dynamic range of ADC.

To find cut-off frequency of the filters, I performed measured amplitude of the excitation signal in the pass band using measure function and by sweeping frequency of the generator I found -3dB frequency. From the Figure 19 below you can see simulation result of cut-off frequency for excitation signal.

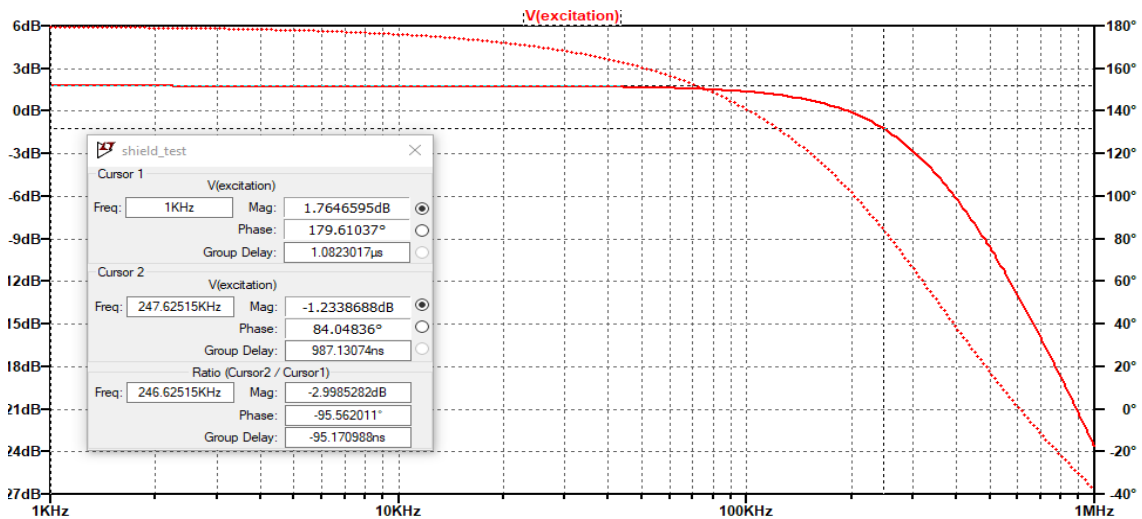


Figure 19. Corner frequency measurement of excitation signal by simulation

As you can see, the simulation result estimates a cut-off frequency of 247 kHz. The peak-to-peak voltage measurement on an oscilloscope at 100 Hz is 2.53 V, and to find the cut-off frequency, I divided 2.53 by square root of 2, which equals 1.79. The frequency that corresponds to this voltage level is 210 kHz, which differs slightly from the simulation result. The main cause of this discrepancy is the inaccuracy of the capacitors and resistors used.

## 5.2 Response filters and inverters

Besides low pass filters in the input side, response signal filters and inverters for differential mode ADC converters are tested with the oscilloscope for 100kHz square wave input, from Figure 20 and Figure 21 below, you can compare results from oscilloscope and simulation.

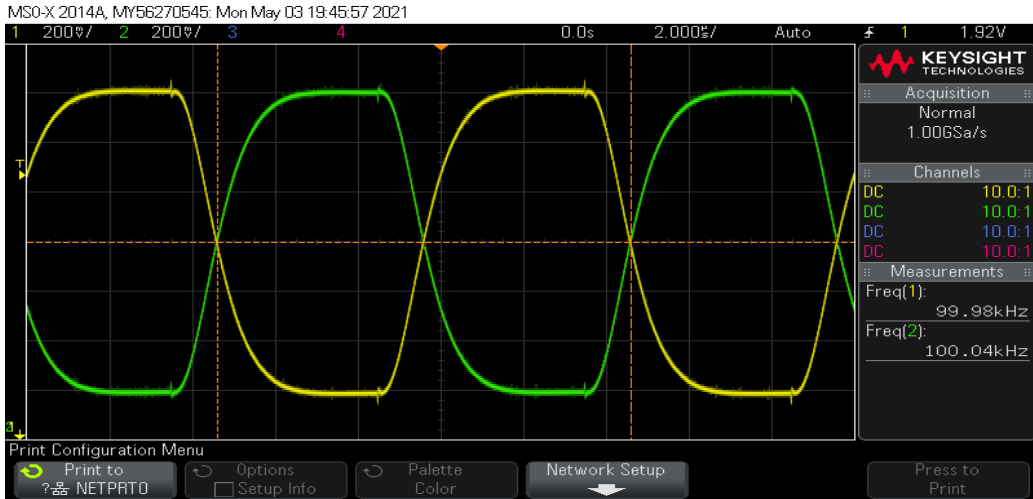


Figure 20. Filtered response signal waveforms for differential ADC inputs, oscilloscope result.

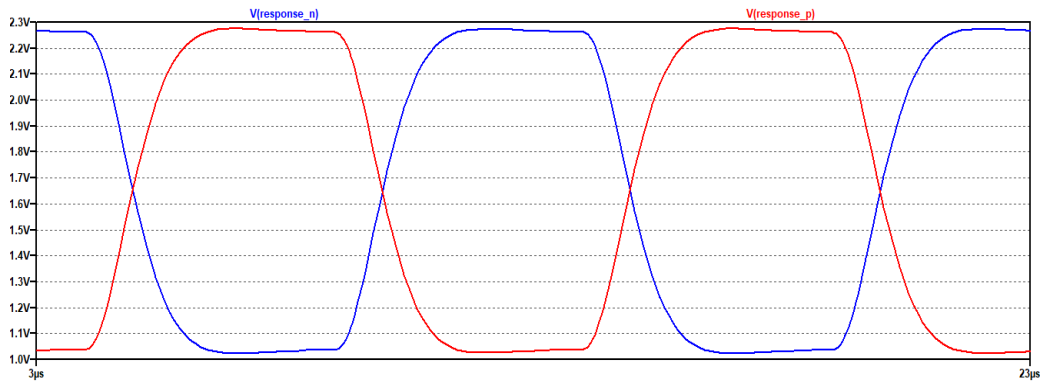


Figure 21. Filtered response signal waveforms for differential ADC inputs, simulation measurement.

These figures confirm proper operations of inverters.

### 5.3 Virtual ground

Furthermore, voltage variations on virtual ground level are measured on oscilloscope and compared with the simulation results. From Table 5, you can compare simulation and oscilloscope results of two different op-amps for voltage variation on virtual ground.

**Table 5. Virtual ground test for different frequencies**

Frequency	V peak-to-peak on virtual ground			
	OPA2350		MCP6022-I/P	
	Simulation	Oscilloscope	Simulation	Oscilloscope
100 KHz	1.17 mV	19 mV	2.25 mV	22 mV
10 MHz	75 mV	127 mV	155 mV	267 mV

Notice that simulation result is significantly different than real measurements, especially at lower frequency. One explanation is that any additional noise increased the peak-to-peak measurement of the oscilloscope, and the other reason is simulation incompleteness. In any case, these values should not be overlooked because they can have an effect on the final calculation.

While ideal source has 0 Ohm series resistance, virtual ground is not ideal, and its series resistance can interfere with measurements. To test resistance of virtual ground, 3.3 V peak-to-peak signal source at 100 kHz and at 10 MHz is connected to the virtual ground through 1kOhm resistor. According to Ohm's law, 3.3 mA ( $3.3 \text{ V} / 1\text{kOhm}$ ) Vpp AC current is supplied, and observer voltage variations are shown in Table 5 above. Now again applying Ohm's law, we can find series resistance of virtual ground at different frequencies. For example, at 10 MHz, the virtual ground circuit made with OPA2350, shows approximately 38 Ohm ( $127 \text{ mV} / 3.3 \text{ mA}$ ). Since virtual ground is connected in series with OUT, we can subtract 38 Ohm from final measured impedance value for specified frequency (10 MHz). Another requirement of this approach is to ensure linearity over applied voltage range. To test linearity, oscilloscope is used in XY mode and voltage level variation at virtual ground (x axis) over 10 MHz alternating current with 3.3mA peak-to-peal value (y axis, 3.3Vpp through 1kOhm resistor) is tested and documented in Figure 22 for OPA2350 and Figure 23 for MCP6022-I/P.

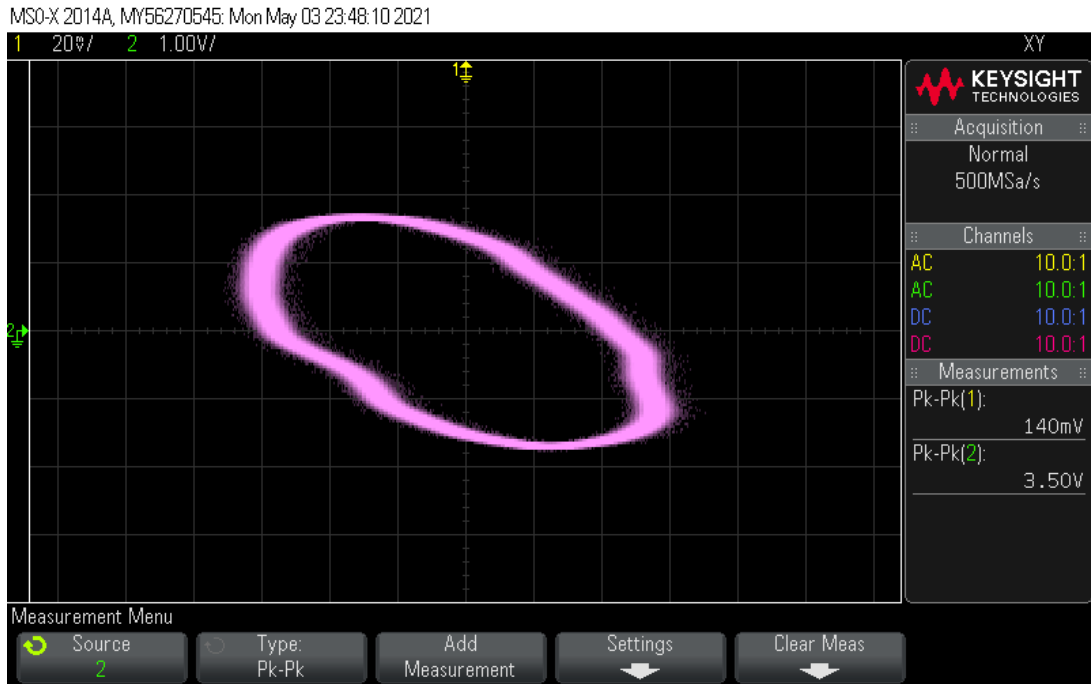


Figure 22. Virtual ground voltage variation at 10 MHz input signal for OP2350

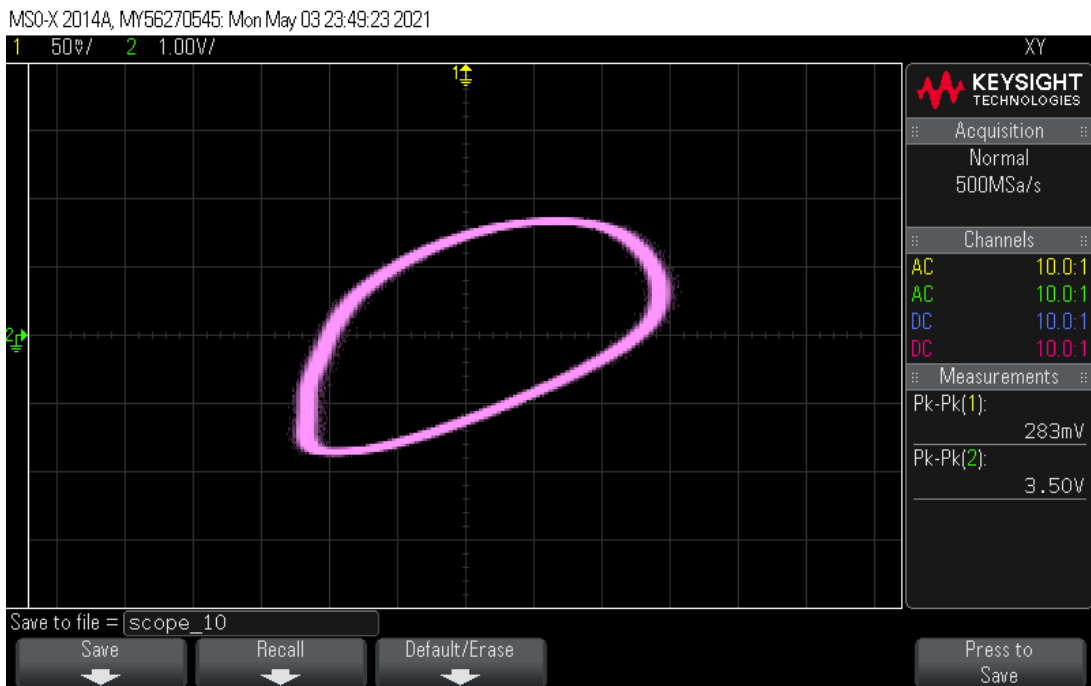


Figure 23. Virtual ground voltage variation at 10 MHz input signal for MCP6022-I/A

These figures show that, phase shift occurs for virtual ground voltage variations in different directions for different op-amps, but more importantly neither of the figures are perfect ellipsis and hence voltage variation in virtual ground is not linear which means

series resistance of virtual ground is not constant even for fixed frequency. As a result, we cannot exactly compensate this resistance from final calculated impedance value but only approximate it. Although OPA2350 reveals lower level of  $V_{pp}$  than MCP6022-I/P at 10 MHz signal thanks to its wider bandwidth, for higher frequency ranges it is not favourable to apply virtual ground approach with these op-amps.

Notice that all oscilloscope waveforms except XY mode outputs provided in this section were obtained with OPA2350 Op-amps, and measurements with the other Op-amp MCP6022-I/P did not vary significantly, except power consumption. During these tests, the OPA2350 Op-amp from Texas Instruments used 30mA on average, while the MCP6022-I/P only used 7mA. While these consumption levels are not excessive and will not impact stationary devices, this disparity must be noted for battery-powered portable devices. The OPA2350, on the other hand, has a broader bandwidth, while the MCP6022-I/P is more cost-effective as well as power-efficient. Overall, there is a trade-off between these options, and the final decision must be based on the application.

## 5.4 ADC and SCI

To measure signals, ADC was set to 16-bit differential mode. To test its output, I used signal generator as input. Sampled result is then sent to the computer over serial communication. Baud rate of 115200 was chosen to provide fast enough communications over reasonable USB cable length. To display result, I used serial plotter feature of Arduino IDE. From Figure 24 below, you can see output of ADC displayed in Arduino serial plotter.

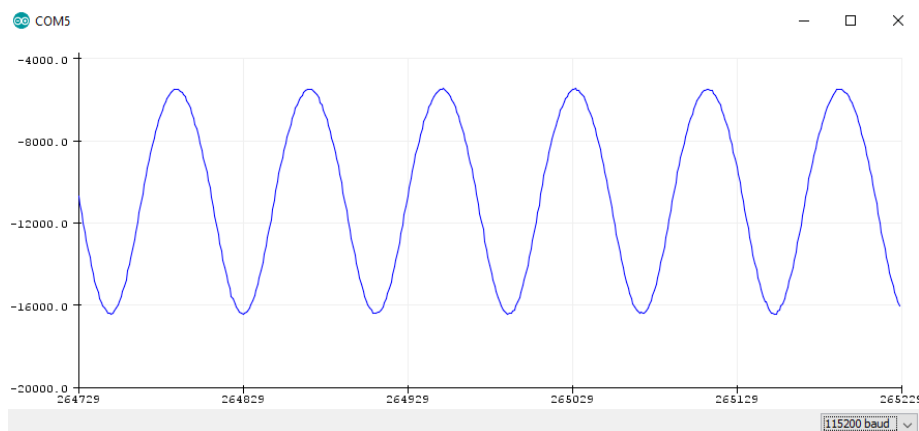


Figure 24. ADC SCI test

As you can see it is possible to get negative value, since differential ADC was used. I also tried to combine HR-PWM code to this one to display internally generated excitation signal but unfortunately some compatibility issues occurred. One possible way to solve this issue can be utilizing the second core which is discussed in the next section along with other future improvements.

## **5.5 Future work**

To obtain a complete, high precision, fast, and reliable impedance spectroscopy system and improve its parameters, some additional tasks must be completed. Missing parts, such as signal generation and sampling integration, as well as the actual implementation of DFT, must be completed in the future. As previously mentioned, it may be advantageous to break some of these tasks between two DSP cores in order to achieve non-interfering code flow. Another benefit of using the second core is that it provides more memory, allowing you to use a larger number of precalculated reference signal values and thus perform impedance spectroscopy at more locations (frequencies).

Another modification that could be made is to use a programmable resistor as a reference resistor. In the current configuration, the reference resistor can be replaced manually from the screw terminal block, but it is possible to measure the OUT value approximately and automatically adjust the resistor to match the OUT. This method allows for greater precision.

Furthermore, though postprocessing impedance value is outside the reach of this thesis, there may be a software interface on the computer side of the link to show results or obtain other useful information from impedance measurements. This graphic interface program can also be used to control the DSP over the computer.

## 6 Summary

In this work, design process of an impedance spectroscopy system based on the TMS320F28069, equipped with features such as external low-pass filters, dc bias removal, high resolution, binary, multifrequency excitation signal, and 16-bit differential ADC was documented.

To meet hardware specifications, PCB add-on was designed, manufactured, and tested. Virtual ground method for removing DC bias was demonstrated to be applicable under the condition that the output impedance of the op-amps be compensated in software. Two separate op-amps were tested for the analog circuit. Although there were no major variations between the two tested op-amps in our case, the OPA2350 op-amp should be used for higher frequencies. Otherwise, the MCP6022/I-P is a better option because it is less expensive, consumes less power, and performs equally well.

On the software side, different modules were examined separately. Individual HR-PWM and 16-bit ADC features have been tested. When both were run on the same CPU, compatibility issues arose. A more in-depth analysis or managing peripherals independently from cores may be used to solve the problem.

Overall cost of the project was kept under 100 euro as planned. The unit is enclosed in plastic to shield it from physical damage and electrical shock, and images of the finished product can be found in Appendix 3.

Finally, the device's developed hardware meets all of the initial specifications, although the software targets were only partially met. As a result, the key issues and causes were explained, and potential solutions were proposed.

## References

- [1] Oliver Heaviside, *The Electrician*, p. 212, 23 July 1886, reprinted as *Electrical Papers*, Volume II, p 64, AMS Bookstore, ISBN 0-8218-3465-7.
- [2] E. Barsoukov and J. Macdonald, *Impedance spectroscopy theory, experiment, and applications*. Hoboken, N.J: Wiley-Interscience, 2005.
- [3] TMS320F2837xD Dual-Core Microcontrollers, Texas Instruments, 2021. [Online]. Available: <https://www.ti.com/product/TMS320F28379D>. [Accessed 15 March 2021].
- [4] 1 MSPS, 12-Bit Impedance Converter, Network Analyzer, AD5933, Analog Devices, 2017. [Online]. Available: <https://www.analog.com/media/en/technical-documentation/data-sheets/AD5933.pdf>. [Accessed 19 April 2021].
- [5] *Impedance Measurement Handbook*, 6.th edition, Keysight, 2020. [Online]. Available: <https://www.keysight.com/zz/en/assets/7018-06840/application-notes/5950-3000.pdf>. [Accessed 2 February 2021].
- [6] P. M. Ramos, F. M. Janeiro, M. TlemÇani and A. C. Serra, "Recent Developments on Impedance Measurements With DSP-Based Ellipse-Fitting Algorithms," in *IEEE Transactions on Instrumentation and Measurement*, vol. 58, no. 5, pp. 1680-1689, May 2009, doi: 10.1109/TIM.2009.2014512.
- [7] T. Radil, P. M. Ramos and A. C. Serra, "DSP Based Portable Impedance Measurement Instrument Using Sine-Fitting Algorithms," 2005 *IEEE Instrumentation and Measurement Technology Conference Proceedings*, 2005, pp. 1018-1022, doi: 10.1109/IMTC.2005.1604294.
- [8] M. Rist, M. Reidla, M. Min, T. Parve, O. Martens and R. Land, "TMS320F28069-based impedance spectroscopy with binary excitation," 2012 5th *European DSP Education and Research Conference (EDERC)*, 2012, pp. 217-220, doi: 10.1109/EDERC.2012.6532258.
- [9] Zhangyong Li, Zhonghua He, Wei Wang, Chaoshi Ren, *Measurement system for electrical impedance and EGG*, Information Technology and Applications in Biomedicine, ITAB 2008. International Conference, 495 – 498.
- [10] F. Gozzini, G. Ferrari and M. Sampietro, "An instrument-on-chip for impedance measurements on nanobiosensors with attoFarad resolution," 2009 *IEEE International Solid-State Circuits Conference - Digest of Technical Papers*, 2009, pp. 346-347,347a, doi: 10.1109/ISSCC.2009.4977450.
- [11] P. Shuquan, "Study on Electrochemical Impedance Response of Sulfate Saline Soil", *International Journal of Electrochemical Science*, pp. 8611-8623, 2019. Available: 10.20964/2019.09.30 [Accessed 1 May 2021].
- [12] *Quadra Impedance Spectroscopy*, Eliko, 2018. [Online]. Available: <https://www.eliko.ee/wp-content/uploads/2016/01/Quadra-Product-Sheet-13.03.2018.pdf>. [Accessed 2 May 2021].



- [13] Z-scope, Scionsoria Electromagnetic Solutions. [Online]. Available: [http://www.scionsoria.com/download/ZSCV62\\_flyer.pdf](http://www.scionsoria.com/download/ZSCV62_flyer.pdf). [Accessed 2 May 2021].
- [14] Precision Impedance Analyzers, 6500B, Issue E, Wayne Kerr Electronics. [Online]. Available: <http://www.waynekerrtest.com/datasheet/instruments/wk6500b.pdf>. [Accessed 3 May 2021].
- [15] OPAx350 High-Speed, Single-Supply, Rail-to-Rail Operational Amplifiers MicroAmplifier Series, Texas Instruments, 2015. [Online]. Available: <https://www.ti.com/document-viewer/OPA2350/datasheet/>. [Accessed 23 April 2021].
- [16] Rail-to-Rail Input/Output, 10 MHz Op Amps, MCP6021/1R/2/3/4, Microchip Technology Inc., 2017. [Online]. Available: <https://ww1.microchip.com/downloads/en/DeviceDoc/20001685E.pdf>. [Accessed 23 April 2021].
- [17] Code Composer Studio integrated development environment (IDE), Texas Instruments. [Online]. Available: <https://www.ti.com/tool/CCSTUDIO>. [Accessed 25 January 2021].
- [18] Code Composer Studio (CCS) Integrated Development Environment (IDE) for C2000 Microcontrollers, Texas Instruments. [Online]. Available: <https://www.ti.com/tool/CCSTUDIO-C2000>. [Accessed 25 January 2021].
- [19] M. Score, "Ceramic or electrolytic output capacitors in DC/DC converters—Why not both?", *Analog Applications Journal*, 2015. [Online]. Available: <https://www.ti.com/lit/an/slyt639/slyt639.pdf>. [Accessed 22 April 2021].
- [20] S. Ghosh, *Signals and Systems*. Don Mills: Pearson Education Canada, 2009.
- [21] A. J. Hinton, B. Sayers, "Impedance Measurement Techniques: Sine Correlation", Solartron analytical, 1998. [Online]. Available: [https://www.ameteksi.com/-/media/ameteksi/download\\_links/documentations/library/solartronanalytical/materials/technical-note-single-sine-correlation.pdf](https://www.ameteksi.com/-/media/ameteksi/download_links/documentations/library/solartronanalytical/materials/technical-note-single-sine-correlation.pdf). [Accessed 1 May 2021].
- [22] M. Min et al., "Binary signals in impedance spectroscopy," 2012 Annual International Conference of the IEEE Engineering in Medicine and Biology Society, 2012, pp. 134-137, doi: 10.1109/EMBC.2012.6345889.
- [23] O. Martens, R. Land, M. Min, P. Annus and M. Rist, "Impedance Measurement Solution Based on the High Time Resolution DSP," 2020 IEEE International Instrumentation and Measurement Technology Conference (I2MTC), 2020, pp. 1-5, doi: 10.1109/I2MTC43012.2020.9128843.
- [24] J. Karki, "Active Low-Pass Filter Design", AAP Precision Analog, Texas Instruments, 2002. [Online]. Available: <https://www.ti.com.cn/cn/lit/an/sloa049b/sloa049b.pdf>. [Accessed 19 April 2021].
- [25] *Analog Applications Journal* 2Q 2015, Texas Instruments. [Online]. Available: <https://www.ti.com/lit/pdf/slyt631>. [Accessed 17 April 2021].
- [26] BoosterPack Resource Kit. [Online]. Available: <https://www.element14.com/community/docs/DOC-55584?ICID=knobe-byob-resourcekit>. [Accessed 15 April 2021].
- [27] *Principles of Data Acquisition and Conversion*, Texas Instruments, 2015. [Online]. Available: <http://www.ti.com/lit/an/sbaa051a/sbaa051a.pdf>. [Accessed 1 May 2021].
- [28] S. B. Kristian, "Differential and Single-Ended ADC", Microchip Technology Inc., 2019. [Online]. Available: <https://ww1.microchip.com/downloads/en/DeviceDoc/Differential-and-Single-Ended-ADC-WhitePaper-DS00003197A.pdf>. [Accessed 2 May 2021].

## **Acknowledgment**

The author would like to acknowledge Dora Plus scholarship that financially supported him during this study.

## **Appendix 1 – Non-exclusive licence for reproduction and publication of a graduation thesis<sup>1</sup>**

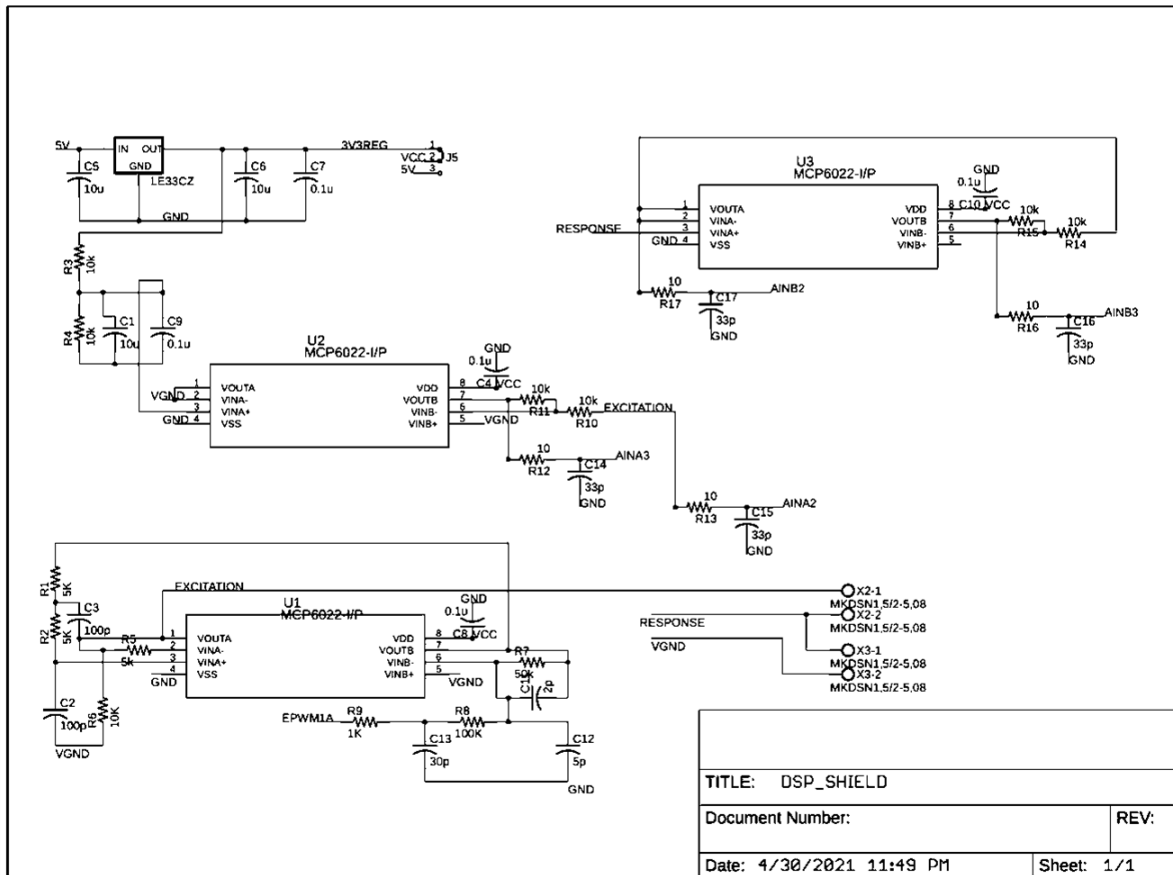
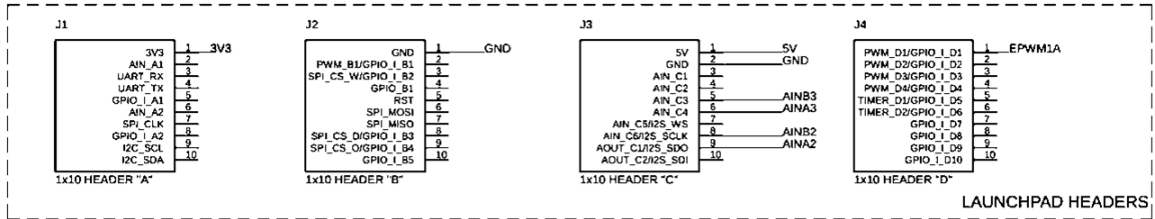
I Anar Abdullayev,

1. Grant Tallinn University of Technology free licence (non-exclusive licence) for my thesis “DSP-based Impedance Spectroscopy Device”, supervised by Olev Martens
  - 1.1. to be reproduced for the purposes of preservation and electronic publication of the graduation thesis, incl. to be entered in the digital collection of the library of Tallinn University of Technology until expiry of the term of copyright;
  - 1.2. to be published via the web of Tallinn University of Technology, incl. to be entered in the digital collection of the library of Tallinn University of Technology until expiry of the term of copyright.
2. I am aware that the author also retains the rights specified in clause 1 of the non-exclusive licence.
3. I confirm that granting the non-exclusive licence does not infringe other persons' intellectual property rights, the rights arising from the Personal Data Protection Act or rights arising from other legislation.

---

<sup>1</sup> The non-exclusive licence is not valid during the validity of access restriction indicated in the student's application for restriction on access to the graduation thesis that has been signed by the school's dean, except in case of the university's right to reproduce the thesis for preservation purposes only. If a graduation thesis is based on the joint creative activity of two or more persons and the co-author(s) has/have not granted, by the set deadline, the student defending his/her graduation thesis consent to reproduce and publish the graduation thesis in compliance with clauses 1.1 and 1.2 of the non-exclusive licence, the non-exclusive license shall not be valid for the period.

# Appendix 2 – PCB schematic



## Appendix 3 – Final prototype

